

Accepted Manuscript

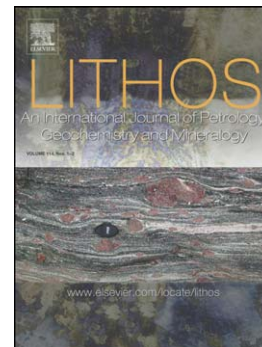
Pre-Alpine contrasting tectono-metamorphic evolutions within the Southern Steep Belt, Central Alps

Manuel Roda, Michele Zucali, Zheng-Xiang Li, Maria Iole Spalla, Weihua Yao

PII: S0024-4937(18)30122-1
DOI: doi:[10.1016/j.lithos.2018.03.025](https://doi.org/10.1016/j.lithos.2018.03.025)
Reference: LITHOS 4617

To appear in: *LITHOS*

Received date: 11 January 2018
Revised date: 29 March 2018
Accepted date: 30 March 2018



Please cite this article as: Roda, Manuel, Zucali, Michele, Li, Zheng-Xiang, Spalla, Maria Iole, Yao, Weihua, Pre-Alpine contrasting tectono-metamorphic evolutions within the Southern Steep Belt, Central Alps, *LITHOS* (2018), doi:[10.1016/j.lithos.2018.03.025](https://doi.org/10.1016/j.lithos.2018.03.025)

This is a PDF file of an unedited manuscript that has been accepted for publication. As a service to our customers we are providing this early version of the manuscript. The manuscript will undergo copyediting, typesetting, and review of the resulting proof before it is published in its final form. Please note that during the production process errors may be discovered which could affect the content, and all legal disclaimers that apply to the journal pertain.

Pre-Alpine contrasting tectono-metamorphic evolutions within the Southern Steep Belt, Central Alps

Manuel Roda^a, Michele Zucali^a, Zheng-Xiang Li^b, Maria Iole Spalla^a,
Weihua Yao^b

^a*Universita' degli Studi di Milano, Dipartimento di Scienze della Terra, Via Mangiagalli
34, 20133 - Milano (Italy)*

^b*The Institute for Geoscience Research (TIGeR), ARC Centre of Excellence for Core to
Crust Fluid Systems (CCFS), School of Earth and Planetary Sciences, Curtin
University, GPO Box U1987, Perth, WA 6845, Australia*

Abstract

In the Southern Steep Belt, Italian Central Alps, relicts of the pre-Alpine continental crust are preserved. Between Valtellina and Val Camonica, a poly-metamorphic rock association occurs, which belongs to the Austroalpine units and includes two classically subdivided units: the Languard-Campo nappe (LCN) and the Tonale Series (TS). The outcropping rocks are low to medium grade muscovite, biotite and minor staurolite-bearing gneisses and micaschists, which include interlayered garnet- and biotite-bearing amphibolites, marbles, quartzites and pegmatites, as well as sillimanite-bearing gneisses and micaschists. Permian intrusives (granitoids, diorites and minor gabbros) emplaced in the metamorphic rocks. We performed a detailed structural, petrological and geochronological analysis focusing on the two main lithotypes, namely, staurolite-bearing micaschists and sillimanite-bearing paragneisses, to reconstruct the Variscan and Permian-Triassic his-

Email address: manuel.roda@unimi.it ()

tory of this crustal section. The reconstruction of the tectono-metamorphic evolution allows for the distinction between two different tectono-metamorphic units during the early pre-Alpine evolution (D1) and predates the Permian intrusives, which comprise rocks from both TS and LCN. In the staurolite-bearing micaschists, D1 developed under amphibolite facies conditions ($P=0.7-1.1$ GPa, $T=580-660^{\circ}\text{C}$), while in the sillimanite-bearing paragneisses formed under granulite facies conditions ($P=0.6-1.0$ GPa, $T>780^{\circ}\text{C}$). The two tectono-metamorphic units coupled together during the second pre-Alpine stage (D2) under granulite-amphibolite facies conditions at a lower pressure ($P=0.4-0.6$ GPa, $T=620-750^{\circ}\text{C}$) forming a single tectono-metamorphic unit (Languard-Tonale Tectono-Metamorphic Unit), which comprised the previously distinguished LCN and TS. Geochronological analyses on zircon rims indicate ages ranging between 250 and 275 Ma for D2, contemporaneous with the emplacement of Permian intrusives. This event developed under a high thermal state, which is compatible with an extensional tectonic setting that occurred during the exhumation of the Languard-Tonale Tectono-Metamorphic Unit. The extensional regime is interpreted as being responsible for the thinning of the Adriatic continental lithosphere during the Permian, which may be related to an early rifting phase of Pangea.

Keywords: Austroalpine Domain, geochronology, multiscale petrostructural analysis, Permian-Triassic extensional tectonics, Variscan convergence

1. Introduction

The European Alps are characterised by structural, metamorphic, sedimentary and igneous signatures that have experienced recurring tectonic and metamorphic rejuvenation during consecutive convergent and divergent plate dynamics since the Cambrian-Ordovician Periods (Schaltegger, 1994; von Raumer et al., 2013, and refs therein). The Alpine nappes originated from continental and oceanic crustal slices, which constituted tectonic units disrupted and reassembled during successive mountain building processes. One of these orogenic events was responsible for the formation of the Variscan chain prior to the Pangaea breakup.

In the Alps, the end of the Variscan orogenic event (ca. 300-290 Ma) is characterised by a high-temperature, low-pressure metamorphic evolution, which is associated with the emplacement of anatectic granitoids (Spalla and Marotta, 2007; Spalla et al., 2014; Schuster et al., 2001, and refs therein). This late orogenic high thermal regime is well known at the scale of the whole European Variscan belt (e.g., Lardeaux, 2014; Lardeaux et al., 2014). The Permian-Triassic high thermal regime in the Alpine area is peculiar because a widespread HT metamorphism affected the Austroalpine and Southalpine continental crust. The resulting high-temperature metamorphism and the associated acidic and mafic igneous activity is long-lasting (from lower Permian to Norian, Spalla et al., 2014) and accompanied by extensional tectonics (Brodie et al., 1989; Lardeaux and Spalla, 1991; Diella et al., 1992; Handy et al., 1999; Schuster et al., 2001). Such a high T/P ratio has been interpreted as being the consequence of lithospheric thinning at the beginning of the Mesozoic continental rifting (Lardeaux and Spalla, 1991; Diella et al., 1992;

Dal Piaz, 1993; Schuster et al., 2001; Marotta and Spalla, 2007; Schuster and Stüwe, 2008; Spalla et al., 2014; Marotta et al., 2018), and the heterogeneous distribution of igneous and metamorphic rocks of this age suggests that the rifting was asymmetric. This interpretation has been supported by the gradual transition from Permian-Triassic metamorphic and igneous ages in the continental crust, to the Mesozoic ages of the ophiolitic remnants (Marotta et al., 2009), and by the long-lasting extensional event that is characterised by regional scale normal faulting during the Permian-Jurassic Periods (e.g., Bertotti et al., 1993).

In the axial zone of the Alps, the recognition of and separation between the Late-Variscan and Permian-Triassic structural and metamorphic signatures are difficult due to the pervasive reworking of the continental lithosphere during the Alpine subduction and collision. The Austroalpine Domain is marked by the occurrence of structural and metamorphic imprints of Variscan convergent tectonics and Permian-Triassic extensional tectonics, being the first one dominant in the Eastern Alps and the second in the western portion of the Austroalpine Domain (Spalla and Marotta, 2007; Marotta et al., 2009; Spalla et al., 2014, and refs therein).

In the Austroalpine crust of Central Alps, the lack of the strong Alpine eclogitisation that characterises the Western Austroalpine Domain (e.g., Polino et al., 1990; Spalla et al., 1996; Bousquet et al., 2004; Gerya and Stöckhert, 2006; Roda et al., 2012; Lardeaux, 2014; Regis et al., 2014) and the concurrent occurrence of widespread mafic to acid Permian intrusions (Gazzola et al., 2000; Zucali, 2001; Spalla et al., 2003; Gosso et al., 2004; Spalla and Zucali, 2004; Salvi et al., 2010; Petri et al., 2016, 2017) make this portion

of the pre-Alpine crust suitable for investigating the relationships between the Variscan and Permian-Triassic tectono-metamorphic evolutions, which is completed after the subtraction of Alpine structural and metamorphic reworking. The results of detailed structural, petrological and geochronological investigations of the Austroalpine crust that is verticalised in the Southern Steep Belt (Schmid et al., 1996) are presented here with the aim to discriminate the interweaving of pre-Alpine convergent and divergent tectonics.

2. Geological setting

The studied poly-metamorphic rock association is located in the Austroalpine Domain of the Central Alps, which is located between upper Valtellina and Val Camonica (Fig. 1). This area belongs to the Austroalpine Domain of the Alps, which occupies the uppermost structural level in the Alpine system and is generally considered to have originated from the Adria plate (Dal Piaz, 2010, and refs therein). The investigated area is part of the Languard-Tonale Tectono-Metamorphic Unit (Salvi et al., 2010), which is historically divided into two lithostratigraphic units: the Languard-Campo nappe (LCN) and Tonale Series (TS). The Tonale Series outcrops from Bellinzona to Passo del Tonale, which is immediately north of the Periadriatic Lineament (Insubric) fault system and it is separated from the LCN to the north by the Mortirolo Line (Werling, 1992; Viola et al., 2003; Meier, 2003). Both units display a steeply dipping attitude (Southern Steep Belt, SSB) and have been attributed to the Middle Austroalpine Domain (Bigi et al., 1990; Schmid et al., 1996; Dal Piaz, 2010). Together with the Grosina Nappe, the Languard-Tonale Tectono-Metamorphic Unit (LCN and TS) is

considered to be the intermediate tectonic element of the Austroalpine Domain of the Central Alps, which overlaps the Lower Austroalpine (Margna, Sella and Bernina) nappes and underlies the Upper Austroalpine (Ortler-Ela) nappe (Mohn et al., 2011).

A Variscan amphibolite facies metamorphic event has been documented for the TS (Braga et al., 2007; Langone et al., 2011), LCN (Braga et al., 2001; Zucali, 2001; Gosso et al., 2004; Spalla and Zucali, 2004; Salvi et al., 2010; Petri et al., 2016), Bernina (Büchi, 1994) and Margna (Guntli and Liniger, 1989) nappes. The LCN consists of low to medium grade muscovite-biotite- and staurolite-bearing gneisses and micaschists with interlayered amphibolites, marbles, quartzites and pegmatites. The TS consists of higher grade sillimanite-bearing gneisses and micaschists, garnet- and biotite-bearing amphibolites, marbles and pegmatites (Bonsignore and Ragni, 1966; Venzo et al., 1971; Gazzola et al., 2000; Spalla et al., 2005). Several post-Variscan acidic and basic intrusives (granitoids, diorites and minor gabbros) occur in both units (Knig, 1964; Bonsignore and Ragni, 1966, 1968; Venzo et al., 1971; Del Moro et al., 1981; Bockemuhl and Pfister, 1985; Tribuzio et al., 1999; Petri et al., 2017). The mineral ages of these igneous rocks span over two time intervals: the first ranges from 300 to 260 Ma (white mica and biotite Rb/Sr; plagioclase and amphibole Rb/Sr and Sm/Nd; zircon U/Pb) and has been interpreted as igneous cooling ages, and the second ranges from 125 to 78 Ma (biotite Rb/Sr) and represents Cretaceous re-activation during Alpine tectonics (Del Moro et al., 1981; Del Moro and Notarpietro, 1987; Gazzola et al., 2000).

The present day lithostratigraphy of the Austroalpine Domain of the Cen-

tral Alps has been interpreted as an inherited character from the Adriatic-European divergent active margin during the Middle Triassic Period, which predates Jurassic rifting (Mohn et al., 2012). According to these authors, the Late Triassic-Early Jurassic stretching, thinning and necking that is related to the Alpine Tethys rifting would have resulted in ductile decoupling and exhumation of the upper portion of LCN (Campo Unit, Froitzheim et al., 1994) along detachment faults from middle crustal levels.

The LCN and TS have long been considered to be heterogeneously affected by an Alpine metamorphic imprint that never exceeded greenschist facies conditions (e.g., Del Moro et al., 1981; Bockemuhl and Pfister, 1985; Froitzheim et al., 1994). However, since the late 1990s, higher-pressure conditions have been identified for the Alpine metamorphism (Spalla et al., 1995; Gazzola et al., 1997, 2000; Zucali et al., 2002; Gosso et al., 2004). The P-T-d-t path for the Alpine event is characterised by a low T/depth ratio during burial (ca. 17°C/km) and exhumation, which is common to both the LCN and TS (Gazzola et al., 2000; Zucali, 2001), and this makes the existing lithostratigraphic subdivision trivial with respect to variations in their tectono-thermal Alpine records. A tectonic re-activation during the Eocene-Oligocene Period along the Periadriatic Lineament and adjacent fault systems (i.e., pseudotachylites belonging to the Mortirolo Line) was reported by Mancktelow et al. (1999).

3. Working approach

During the evolution of mountain belts, lithospheric slices within the subduction-collision zone are likely to be coupled and decoupled repeatedly

during their trajectories across different structural levels. The effect is a continuous size variation of transient tectonic units that can accrete or disaggregate under different PT conditions and before their final exhumation. Consequently, the orogenic belts are characterised by a highly heterogeneous distribution of structural and metamorphic imprints that makes the reconstruction of tectonic events difficult. Therefore, a working method which enables researchers to recognise distinctive rock units with unique structural and metamorphic histories (the tectono-metamorphic units - TMUs, Spalla et al., 2000; Zucali, 2001; Spalla et al., 2005, 2010; Gosso et al., 2015) is fundamental.

This kind of investigation requires the synergic use of deformation pattern in the field and microstructural analysis to decipher the equilibrium metamorphic assemblages that mark the superposed fabrics, which possibly relates to absolute age data. For this reason, the analytical approach used during this work comprises the following steps: (a) structural mapping that integrates reconstruction of the foliation trajectories with lithostratigraphic analysis; (b) determination of the kinematic compatibilities between superposed structures and their relative chronology at the regional scale to separate the successive deformation stages; (c) individuation of sampling sites that are critical for identifying the mineralogical support of superposed fabrics in different bulk compositions; (d) cross control of fabric and metamorphic assemblage sequences in adjacent volumes that are heterogeneously deformed (from low to high-strain domains); and (e) achievement of thermo-barometric estimates and radiometric dating on mineral phases, which mark the successive fabrics of known relative chronology at the regional scale. The synthesis

of these data leads to the reconstruction of the P-T-d-t paths, which constitute the basic reference for the individuation of TMUs which corresponds to the volumes that underwent the same PT history during the same time interval.

4. Lithostratigraphy

Although several rocks characterise the LCN and TS, we focused the detailed structural and metamorphic analysis on two main rock types, namely, staurolite-bearing micaschists and sillimanite-bearing paragneisses (Fig. 2). We select these rocks because the weak Alpine metamorphism recorded by those lithologies makes the reconstruction of the pre-Alpine structural and metamorphic evolution more effective. Both rocks outcrop within the LCN and TS and show a pre-Alpine polyphasic metamorphic evolution. The occurrence of Permian intrusives (Figs 2 and 3) facilitates the distinction between Alpine and pre-Alpine structures and metamorphic imprints because they were deformed together with the LCN and TS country rocks during the Alpine convergence.

Staurolite-bearing micaschists consist of medium to fine-grained rocks with a discontinuous foliation that is defined by alternate films and lithons (Fig. 3a). Films are composed of white mica and biotite with shape preferred orientation (SPO) that is parallel to the mineral layering. Lithons are composed of a quartz and plagioclase aggregate. Staurolite, garnet and kyanite porphyroblasts are common within lithons and are wrapped by mica films. Even though staurolite and kyanite grains generally lie within the main foliation, they do not mark the mineral lineations (Fig. 3a). Mica-rich

films mark a spaced foliation, which is discontinuous to quasi-continuous, and mica-layers generally range in size from mm to cm. White mica may also occur as cm-sized single flakes, while biotite never exceeds 0.5 cm. Dark thin aggregates of Alpine chloritoid rim staurolite porphyroblasts or overgrow them. Two different types of chlorite occur. An alpine chlorite rims the aggregates of pre-Alpine (garnet and staurolite) and Alpine HP minerals (chloritoid, garnet and white micas) and an early chlorite that lies within the main foliation.

Sillimanite-bearing paragneisses mainly consist of medium to fine-grained, brownish coloured gneisses, which are characterised by anastomosed and discontinuous foliation, marked by biotite and sillimanite-rich films that alternate with quartz and K-feldspar-rich lithons (Fig. 3b). Biotite-rich layers vary in thickness from mm to 1 cm; sillimanite may occur as white-greyish aggregates, which are a few mm-thick and 2-3 cm long. Lithons generally consist of quartz, K-feldspar, plagioclase, garnet and locally, biotite (Fig. 3b and c). Garnet porphyroblasts generally display a euhedral shape and brownish colour (Fig. 3c); in places, the aspect ratio of garnets reaches up to 3, with the longer side generally parallel to the main foliation; and biotite inclusions may define an internal foliation that is oblique to the external foliation.

5. Meso and micro-structural evolution

The heterogeneity of the finite deformation field that affects the studied area preserves different domains, in which the fabric of single deformation stage is dominant (Zucali, 2001; Gosso et al., 2004; Salvi et al., 2010). Con-

sequently, we selected domains with dominant pre-Alpine fabrics, and we collected samples that preserve the largest volume of rock characterised by mineral associations in equilibrium with the successive tectono-metamorphic stages.

Within the two rock types, four main groups of superimposed meso-microstructures may be separated on the basis of geometrical and kinematic compatibility analysis and mineral associations (Figs 2, 3 and 4). Mineral abbreviations are according to Whitney and Evans (2010). As a function of their relations with Permian intrusives the D1 and D2 stages can be distinguished as pre-Alpine and D3 and D4 as Alpine. The Alpine re-equilibration affects all lithotypes although with different degrees of deformation, from coronitic to mylonitic textures (Spalla et al., 1995; Gazzola et al., 1997, 2000; Zucali, 2001; Gosso et al., 2004). The first Alpine structure (D3, Figs 2 and 4) is characterised by a foliation (S3, Gazzola et al., 2000) that occurs as the axial plane associated with D3 folds or within the shear zones in the micaschists and paragneisses, and this is marked by SPO of Wm, Qz and locally of Ctd. Grt and Ctd generally occur within lithons as porphyroblasts up to 1 cm in size. D4 structures (Gazzola et al., 2000) consist of folds and m-scale shear zones (Figs 2 and 4). D4 folds bend pre-existing foliations and develop from cm-scale crenulations to m-scale isoclinal folds. SPO of Wm, Chl, Qz and rare green Bt marks the S4 foliation.

Within the coronitic domains of staurolite-bearing micaschists and sillimanite-bearing paragneisses, D1 and D2 pre-Alpine structures can be detected. D2 dominates both lithotypes, and it is characterised by a variably continuous S2 foliation. The D1 structures can be distinguished within lithons of

S2 foliation and are characterised by a composite S1 foliation that is from spaced to continuous. The mineral association marking the S1 foliation in the staurolite-bearing micaschists is different from that in the sillimanite-bearing paragneisses, but no overprinting relationships have been detected between the two foliations (Fig. 2). For this reason, we distinguish a D1a stage that is characterised by an S1a foliation within the staurolite-bearing micaschists, and a D1b stage that is characterised by an S1b foliation within the sillimanite-bearing paragneisses. In the following sections, we focus on the pre-Alpine evolution.

5.1. Pre-Alpine evolution

5.1.1. Stage D1a

At the mesoscale, the first pre-Alpine deformation and metamorphic event in the staurolite-bearing micaschists (D1a, M1a, Figs 2 and 3, Table 1) is characterised by a discontinuous foliation that is marked by mm- to cm-thick layers rich in St-Bt-Grt and Qz-Kfs-Pl (S1a, Fig. 3a). At the microscale, S1a is a relict foliation that is up to mm-thick within the S2 films or is preserved in metre-sized lenses, which escaped the D2 deformation phase. S1a is marked by SPO of Wm1a, Bt1a and St (Fig. 5a) and is alternating mm-thick Qz-rich and feldspars lithons, which contain Grt1a porphyroblasts (Fig. 5b). Alpine garnets (Grt_{ALP}) often grow as coronae on Grt1a (Fig. 5b). Wm1a and Bt1a occur as mm-sized grains with undulose extinction (Fig. 5b). St occurs as single grains that are mm- to cm-sized with undulose extinction, subgrains and irregular grain boundaries (Fig. 5c). Porphyroblasts of Grt1a have reaction rims and locally, they are characterised by an internal foliation that is marked by grains of Ilm and Turm. Qz has undulose extinction, subgrains

and irregular grain boundaries. Rare relicts of Ky may occur within the S1a foliation (Fig. 5a).

Consequently, the assemblage that is interpreted as stable during stage D1a in the staurolite-bearing micaschists is as follows (Table 1): Bt1a + St + Wm1a + Grt1a + Pl + Qz + Ilm + Tur \pm Rt \pm Ky \pm Kfs

5.1.2. Stage D1b

In the sillimanite-bearing paragneisses, D1b consists of a discontinuous foliation, which is marked by layers rich of Sil-Bt-Grt and Qz-Kfs-Pl assemblages (S1b, Fig. 3b). At the microscale, S1b is a rather continuous foliation, which is marked by SPO of Bt1b, Sil1 and Qz aggregates (Fig. 6a, b), as well as by mm to cm-thick lithons that alternate with Qz and Kfs-rich and Bt-rich layers. Bt1b occurs as mm-sized grains with brownish pleochroism and an undulose extinction (Fig. 6c). Sil1 occurs as prismatic mm-sized grains with irregular boundaries and locally with an undulose extinction (Fig. 6b, d). Qz has an undulose extinction, deformation bands, subgrains and irregular grain boundaries. Porphyroblasts of Grt1b have a regular shape and locally, they have an internal foliation, which is marked by Bt and fibrolitic Sil. Bt1b, Sil1 and Grt1b are characterised by rational boundaries. Locally, mm-sized grains of Crd, which are twinned and have yellowish pleochroism, occur within Qz-Pl, and the skeletal grains of Wm (pre-D1b) are partially replaced by Sil1.

Consequently, the assemblage that is interpreted as synchronous with stage D1b in the sillimanite-bearing paragneisses is as follows (Table 1): Bt1b + Sil1 + Grt1b + Pl + Qz + Ilm \pm Rt \pm Kfs \pm Crd.

5.1.3. Stage D2

The D2 stage is shared by both lithotypes and is generally represented by the S2 foliation, well preserved within both rocks and marked by SPO of Bt, Sil and Qz (Figs 3 and 4). D2 deformation may even be represented by cm to dm-thick, tight to isoclinal folds. D2 is mostly recorded as crenulation of S1. D2 folds may have a m to 100 m-scale wavelengths; the fold axial plane (AP2) generally shows an east-west strike and variable dipping values, while A2 fold axis has variable attitudes (Fig. 2); S2 generally reproduces the AP2 attitudes, which shows a cluster of poles to planes along the north-south direction (Fig. 2). S2 is the most pervasive foliation and S1 is locally preserved in up to cm- thick relicts. Rare cm-sized Grt in sillimanite-bearing paragneisses retains an internal foliation, which is marked by Bt1b and shows a high angle with respect to S2 (Fig. 3b).

Although S2 is generally common between the two rocks, some small differences occur at the microscale. S2 in the staurolite-bearing micaschists is marked by SPO of Bt2, Sil2, Qz and Pl aggregates and partially reactivates S1a foliation at a low angle. Bt2 occurs as mm-sized brownish grains that wrap the Wm1 and Bt1 levels. Sil2 occurs as a garben of fibrolite needles (Fig. 5b). Pl is locally sub-millimetric in size with deformation twins. In the sillimanite-bearing paragneisses, the S2 foliation is generally a crenulation cleavage marked by SPO of Bt2 and Sil2 in alternation with levels of Qz, Pl and Kfs. Bt2 is sub-millimetric in size with an anhedral habit and weak pleochroism. As with the staurolite-bearing micaschists, Sil2 occurs as a garben of fibrolite needles that wraps Bt1b, Sil1b and Grt1b (Fig. 6d). Locally, Sil2 shows a pseudomorphic replacement by Alpine Ky, Wm and

Chl.

Consequently, the assemblages interpreted as stable during stage 2 are (Table 1): i) $\text{Bt}_2 + \text{Sil}_2 + \text{Pl} + \text{Qz} + \text{Tur} \pm \text{Grt}_{1a} \text{ rim} \pm \text{Crd}$ in the staurolite-bearing micaschists and ii) $\text{Bt}_2 + \text{Sil}_2 + \text{Pl} + \text{Ilm} + \text{Qz} + \text{Tur} \pm \text{Grt}_{1b} \text{ rim} \pm \text{Crd}$ in the sillimanite-bearing paragneisses.

D1 and D2 fabrics are never recorded in Permian intrusives; igneous contacts between intrusives and the country rocks are only locally preserved (Fig. 3d) and are often reworked during Alpine polyphase tectonics. Some intrusives may occur within 10 cm-sized tension-gashes at a high angle with respect to S2, or they may show fuzzy contacts with gneisses and schists that are foliated by S2 (Fig. 4a). These characters suggest a syn-D2 emplacement of the intrusives. In the sillimanite-bearing paragneisses, rare growth of Spl, Crn and Bt_{2_1} may occur within the Sil1 boudin necks. The time relationship of this boudinage is still unclear. The assemblage usually occurs within rocks close to small dioritic intrusions. For this reason, this event is interpreted as the result of a local high temperature contact metamorphism.

5.2. Stage post-2

No tectonic fabric is associated with this event. At the microscale, the post-2 event is marked only by rare And (Fig. 5d) and Wm2 porphyroblasts, which overgrow S1 and S2 within both lithotypes. The assemblage that is stable during this stage is as follows (Table 1): $\text{Wm}_2 + \text{Qz} + \text{Tur} \pm \text{And}$.

6. Mineral chemistry

We detected the mineral compositions for selected microstructural sites, which were chosen for their potential to reveal the transformation path-

ways that accompany fabric evolution, as well as to support the thermo-barometric estimates and pressure-temperature path reconstruction. Representative mineral analyses from staurolite-bearing micaschists (9 samples) and sillimanite-bearing paragneisses (6 samples) are shown in Tables 2 and 3, respectively. Compositional variations are detailed in Tables 4 and 5 and illustrated by diagrams (Figs 7, 8 and 9). They show the compositional trends for the principal mineral phases that are diagnostic for thermo-barometric estimates.

6.1. Staurolite-bearing micaschists

Biotites of staurolite-bearing micaschists show different amounts of Ti, which are a function of their equilibrium stage. From stage D1a (S1a) to stage D2 (S2), the Ti content slightly increases, while a remarkable decrease occurs together with a decrease in the X_{Mg} content during Alpine stages (Table 3 and Fig. 7a, b). Garnet 1a zoning, from core to rim, is characterised by an increase in Ca (Fig. 8a, c) and a consequent decrease in Fe (Fig. 8a, c). The coronae developed on Grt1a have an amount of Ca and Fe that is similar to Alpine garnets (Grt_{ALP}, Fig. 8a, c). No sensible variation of Mg and Mn has been detected for garnets during pre-Alpine stages (Fig. 8b, d). During the different metamorphic stages, from D1a to D3, Wm shows a remarkable increase in the amount of Mg and Si and a decrease in the Al_{tot} content (Fig. 9a, b). A small decrease in Pg content is also observable from D1a to D3 (Fig. 9c).

St is characterised by a low amount of Mg (from 0.06 to 0.21 apfu) and Zn (from 0.01 to 0.89 apfu). Pl compositions vary from andesine to albite as a function of the progress of Alpine re-equilibration, (Table 4) and Kfs

is anorthoclase in composition. Fe^{2+} content in Ilm varies from 0.81 to 1.00 apfu (Table 4).

6.2. Sillimanite-bearing paragneisses

The amount of Ti in the Bt of sillimanite-bearing paragneisses (Fig. 7c, d) decreases from stage D1b (S1b) to stage D2. Bt_{21} shows a low Ti content and a relatively high Al_{tot} (Fig. 7c, d). Garnets do not show chemical differentiation during pre-Alpine stages (Fig. 8e, f, g, h). In contrast, during the Alpine stages, garnets show a strong increase in Ca and Mg content and a decrease in the amount of Fe (Fig. 8e, f, g, h). Pre-Alpine skeletal Wm_{pre1b} has a low Mg content and a relatively high Al_{tot} , while Alpine Wm shows an increase in the amount of Mg and a decrease in the Al_{tot} (Fig. 9d, e). No remarkable variation in Pg content has been detected between pre-Alpine and Alpine micas (Fig. 9f).

Pl compositions vary from bytownite to oligoclase as a function of Alpine re-equilibration, and the anorthite content is generally higher than that of Pl in staurolite-bearing micaschists (Table 5). Kfs have a sanidine composition. Fe^{2+} content in Ilm varies from 0.76 to 0.96 apfu (Table 5). Crd has Mg and Fe^{2+} of 0.90 and 0.55 apfu, respectively. Fe^{2+} content in Spl ranges between 0.55 and 0.82 apfu and it is compositionally classified as Hercynite (Table 5).

7. Pressure and temperature conditions of metamorphism

Microstructural analysis indicates that the investigated rocks preserve evidence of superposed structural and metamorphic re-equilibrations (even in volumes as small as a thin section), and this allows the individuation

of paragenetic sequences. Microstructural analysis also permits the identification of favourable sites where microstructures suggest the attainment of a grain-scale equilibrium (e.g. rational grain boundaries and coeval co-existence suggested by the microstructural analysis) to infer PT conditions during each re-equilibration stage. PT values derived using critical minerals such as garnet, in which the compositional zoning suggests a heterogeneous re-equilibration, have been calculated using mineral pairs that are in mutual contact in textural domains selected using microstructural analysis. In this light, successive physical conditions of metamorphism have been inferred using the following tools: a) the application of well calibrated independent thermo-barometers; b) comparison of natural assemblages with experimental univariant equilibria; c) average PT using the THERMOCALC program (Holland and Powell, 1998); and d) calculation of univariant reaction curves and equilibrium fields using *Perple_X* (Connolly, 2005); in particular, pseudo-sections have been used to constraint PT relative evolution of reconstructed paragenetic sequences more than precise P-T conditions (e.g using isopleths intersections). Following this approach, samples that display a unique structural and metamorphic imprint at the thin section scale yield internally coherent PT estimates. Thermo-barometric estimates and errors are shown in Table 6. PT fields for each event consider the cross-correlation between the results of different applied methods (Figs 10 and 11), and these are supported by the coherence with successive parageneses, which are inferred by microstructural analysis (Table 1).

The bulk rock compositions of sillimanite-bearing paragneisses and staurolite-bearing micaschists were calculated from modal amounts obtained by optical

analysis using comparative charts, averaged with microprobe compositions; PT pseudosections (Fig. 10) were calculated in the simplified model system KFMASH, capable of reconstructing inferred paragenetic sequences, avoiding the addition of Na_2O and CaO since they mainly stabilise plagioclase but not change the topology of the stability fields. Perple_X software (ver. 6.7.2 Connolly, 1990, 2005) was used over the PT range of 0-1.5 GPa and a gridded Gibbs free-energy minimisation approach (Connolly, 2005) was adopted. The thermodynamic database of Holland & Powell (1998, updated 2002, Holland and Powell, 1998, 2001) was used. Solid solution models are Grt(HP) for garnet (Holland and Powell, 1998); Opx(HP) for orthopyroxene (Holland and Powell, 1996); hCrd - Sp(HP) - Bio(HP) for cordierite, spinel and biotite (Powell and Holland, 1999); Pl(h) for plagioclase (Newton et al., 1980); Mica(CHA) for white mica (Coggon and Holland, 2002; Auzanneau et al., 2010); St(HP) - Ctd(HP) for staurolite and chloritoid (White et al., 2000). The fluid phase was assumed to be pure H_2O , which was initially in excess.

Temperature and pressure ranges from ca. 580 to 660°C and ca. 0.7 to 1.2 GPa have been estimated by Perple_X for the assemblage of stage D1a of staurolite-bearing micaschists (Fig. 10a). Independent thermometers suggest a slightly lower temperature range (Table 6), which ranges between 530 and 590°C. In contrast, the average PT estimates performed with THERMOCALC agree with the equilibrium field, which was obtained by Perple_X (Fig. 11 and Table 6). The upper temperature limit is constrained by the stability of St (Spear and Cheney, 1989; Spear, 1993), which marks the S1a foliation, and the lower temperature limit is defined according to the reaction

$\text{Chl} + \text{Ms} = \text{Bt} + \text{Als}$ that was calculated with THERMOCALC. A minimum pressure of 0.7-0.8 GPa has been estimated by independent barometers and by the average PT performed with THERMOCALC (Table 6), which is consistent with the estimates of Perple_X (Fig. 10a).

A temperature range of ca. 750-870°C and a pressure range of ca. 0.5-1.0 GPa have been estimated by Perple_X for the assemblage of stage D1b of sillimanite-bearing paragneisses (Fig. 10b). Textural evidence of biotite instability consists of (a) partial replacement of biotite by sillimanite needles (Fig. 6d), (b) poikiloblast of quartz and feldspar, which accounts for biotite-assisted partial melting. The quite homogeneous compositional profile across garnet cores, which indicates that the composition of these mineral phases cannot be used confidently for thermobarometric estimates of the D1b stage. In addition, a strong re-equilibration involved Bt and Grt during successive metamorphic stages. For these reasons, the estimates from independent thermo-barometers resulted in a lower temperature range (Table 6). A maximum temperature of ca. 720°C is obtained from the Ti content in Bt1b (Henry, 2005) while lower temperature ranges result from contact mineral pairs thermometers and the average PT performed with THERMOCALC (650-660°C, Table 6). A pressure range between 0.4 and 0.6 GPa results from independent barometers (Table 6).

The D2 stage is shared by the two lithotypes and the integration of thermo-barometric estimates, which are obtained with Perple_X for both D2 assemblages, show a temperature range between ca. 620 and ca. 750°C and a pressure range between ca. 0.4 e ca. 0.6 GPa (Fig. 11). Temperatures obtained by Ti content in Bt2 (Henry, 2005) vary between 600 and 690°C

(Fig. 11 and Table 6) and agree with the estimates of Perple_X. The following post-D2 exhumation stage is defined by static growth of And and Wm2; consequently, the relative conditions of post-2 assemblage (Fig. 11) are of $<500^{\circ}\text{C}$ and <0.5 GPa.

Generally, the estimates obtained with different independent thermo-barometers for each metamorphic stage (Table 6) are remarkably similar to each other. They are quite consistent with the PT conditions suggested by the equilibrium fields and obtained with Perple_X (Fig. 10). However, temperatures obtained by independent thermo-barometers lie in the lower range of the Perple_X estimates, especially those obtained by mineral pairs in contact with garnets and generally shows a strong re-equilibration during successive Alpine metamorphic stages.

8. Geochronology

Zircon U-Pb geochronology was conducted on sample 04AP01, which was collected from sillimanite-bearing paragneisses (Fig. 1 for sample location) using the sensitive high-resolution ion microprobe (SHRIMP) facility at the John de Laeter Centre, Curtin University. Zircon grains were extracted from the bulk rock sample using traditional mineral separation techniques (crushing, grinding, water table, magnetic separation and heavy liquids) and were hand-picked and mounted in epoxy resins with zircon U-Pb standards for crystal polishing. All zircon grains were imaged in transmitted and reflected light, as well as cathodoluminescence (CL) to reveal their internal structures. The analyses were carried out in standard operation conditions of 2 nA O₂-primary beam, 20 μm spot size and 5000 mass resolution, and each analysis

consisted of 5 cycles. The U concentration was calibrated using zircon standard CZ3 (Pidgeon et al., 1994), and the $^{206}\text{Pb}/^{238}\text{U}$ ratio was constrained by standard TEMORA1 (Black et al., 2003). The detailed analytical procedure follows that of Williams (1997). For zircons with a clear rim and core boundaries under CL images, spots were placed on rims according to the ages of the metamorphic overgrowths (Fig. 12a-c). Data reduction was carried out using the Squid (Ludwig, 2001b) and Isoplot/Ex (Ludwig, 2001a) packages.

The SHRIMP U-Pb data for sample 04AP01 are presented in Table 7. Twenty-five analyses were conducted on 25 individual zircon grains; of which, 22 analyses concordant U-Pb ages with acceptable common ^{206}Pb values (Table 7). Three zircon grains, where the analytical spots were on or mostly on the zircon cores (Fig. 12d), gave Paleozoic ages (Fig. 12e). These likely represent detrital zircons of the sedimentary protolith. The remaining 19 analyses are all from zircon rims, which commonly show metamorphic sector zoning structures (Fig. 12a-c) and have low Th/U ratios of 0.01-0.20 (Fig. 12f and Table 7); the $^{206}\text{Pb}/^{238}\text{U}$ ages fall in the range of 275-250 Ma, with a dominant peak at 275 Ma (weighted mean 276 ± 2 Ma, $n=10$, $\text{MSWD}=0.49$), and two minor peaks at ca. 265 Ma (weighted mean 264 ± 3 , $n=6$, $\text{MSWD}=0.25$) and ca. 250 Ma (weighted mean 250 ± 4 , $n=3$, $\text{MSWD}=0.10$), respectively (Fig. 12e-h).

9. Discussion

On the basis of the analyses performed on staurolite-bearing micaschists and sillimanite-bearing paragneisses, two main pre-Alpine deformation stages (D1 and D2) and a post-D2 LT-LP metamorphic stage have been recon-

structed. The pre-Alpine D1 stage is characterised by two different fabric relicts (S1a and S1b), which are developed under different metamorphic conditions (Figs 11 and 13). S1a occurs within staurolite-bearing micaschists and developed under amphibolite facies conditions (Fig. 13); it is characterised by a thermal state traditionally interpreted as compatible with a thermal gradient of an old plate or a thickened zone, a bit higher than a stable geotherm of the continental crust ($P=0.7-1.1$ GPa, $T=580-660^{\circ}\text{C}$, Fig. 11). S1b occurs within sillimanite-bearing paragneisses and developed under granulite facies conditions ($P=0.6-1.0$ GPa, $T>780^{\circ}\text{C}$, Fig. 11); it is characterised by a higher thermal state exceeding the maximally relaxed geotherm after a continental collision (Fig. 11).

Therefore, the two deformation stages correspond to significantly different tectonic contexts. S1a fabric in staurolite-bearing micaschists (Barrovian metamorphic imprint) was developed under a thermal gradient typical of a thickened crust during the mature collisional stage, which is widely described in the Southalpine (Diella et al., 1992; Spalla and Gosso, 1999) and Austroalpine Domain (Lardeaux and Spalla, 1991; Spalla et al., 1995) of the Alps and dated ca. 330 Ma in the Southalpine Domain. Syn-D1b PT conditions for the sillimanite-bearing paragneisses supersede the fully relaxed geotherm, which describes a perturbed thermal state with additional heat production from radioactive decay (England and Thomposon, 1984). This requires an extra heat supply, such as asthenospheric upwelling that is compatible with slab and/or orogenic root-delamination after a continental collision, which promotes late orogenic extension (Spalla and Marotta, 2007; Marotta et al., 2009; Spalla et al., 2014). Therefore, the two rock types have

been characterised by different tectono-metamorphic evolutions before the D2 stage. Both lithologies outcrop within the lithostratigraphic units LCN and TS (Fig. 2), making this historic subdivision superseded in this portion of the Central Alps.

To better understand the meaning of the two different pre-D2 stages, we compare their PT estimates with the PT conditions predicted by continental crustal markers of a numerical model of convergence (Regorda et al., 2017), from the oceanic subduction to the continental collision (Fig. 13). D1a fits the conditions predicted by the model in the upper plate during subduction up to the early collisional stages. Conversely, D1b fits the conditions predicted by post-collision stages.

D2 deformation is the earliest common tectonic imprint shared by the two rock types (Fig. 11), under which staurolite-bearing micaschists and sillimanite-bearing paragneisses have been coupled. From this time on, the two contrasting metamorphic rock types formed a single tectono-metamorphic unit and maintained coherence during the subsequent pre-Alpine exhumation and Alpine burial. D2 developed under granulite-amphibolite facies conditions at a relatively low-pressure ($P=0.4-0.6$ GPa, $T=620-750^{\circ}\text{C}$, Fig. 11). The estimated thermal state lies in the field of the Abukuma metamorphic field gradient (Fig. 13). On the basis of structural analyses, the D2 stage is interpreted as contemporaneous with the emplacement of Permian bimodal intrusives, which agrees with Gazzola et al. (2000), Zucali (2001) and Gosso et al. (2004). Geochronological analyses on zircon rims of sillimanite-bearing paragneisses indicate ages ranging between 250 and 275 Ma, which agrees with the ages of intrusives (280-264 Ma, Del Moro et al., 1981; Del Moro and

Notarpietro, 1987; Gazzola et al., 2000). Therefore, the reported metamorphic ages date to the D2 tectono-metamorphic event.

The age of Sondalo gabbro, which occurred within the Austroalpine basement north of the Mortirolo Line, ranges from 300 Ma (early cooling event) to 270 Ma (late cooling event) based on Sm/Nd and Rb/Sr geochronology on norites and troctolites (Tribuzio et al., 1999). The intrusion of the Sondalo gabbroic complex occurred initially at the mid-crustal level (0.5-0.6 GPa) and was progressively exhumed (<0.45 GPa), which generated partial melting of the host rock in the metamorphic aureole (Petri et al., 2016). The U-Pb ages of the zircons from diorites close to the gabbro and from the metamorphic aureole are similar and range between 280 and 290 Ma (Petri et al., 2017). Our data indicates a later metamorphic event in the Languard-Tonale Metamorphic Unit (south of the Mortirolo Line) between 250 and 275 Ma. Therefore, the two crustal portions that are north and south of the Mortirolo Line have been re-equilibrated under similar metamorphic conditions at different times (ca. 285 and 265 Ma, respectively). An anomalously high thermal regime thus affected the Austroalpine crust of the Central Alps for at least 40 Ma. Such a Permian HT-metamorphic imprint, which is interpreted as a consequence of lithospheric thinning, may also affect other sections of the Austroalpine and Southalpine Domains along the Alpine belt (e.g., Brodie et al., 1989; Lardeaux and Spalla, 1991; Diella et al., 1992; Spalla et al., 1995; Handy et al., 1999; Schuster et al., 2001; Schuster and Stüwe, 2008; Marotta et al., 2009; Spalla et al., 2014; Marotta et al., 2018; Petri et al., 2017). Older Paleozoic ages (ca. 380 and 315 Ma) recorded by zircon rims closer to the core (Fig. 12d, e) can correspond to Variscan metamor-

phic re-equilibrations, which agree with the interpretations of the Sondalo country rocks (Petri et al., 2016) based on radiometric data in surrounding Austroalpine units (Thoeni, 1981; Langone et al., 2011, and refs therein). We propose that the exhumation of the Languard-Tonale Tectono-Metamorphic Unit was promoted by lithospheric thinning, which began during the Lower Permian and after the Variscan subduction and collision. The exhumation was assisted by a high thermal state until the post-D2 stage when the static growth of And and Wm occurred. The Permian extensional regime has been interpreted as being responsible for the thinning of the Adriatic continental margin leading up to the Mesozoic breakup of the supercontinent Pangea, which is similar to the Permian and Triassic extensional structures occurring along the north Atlantic margins and pre-dating the opening of the Jurassic Ocean (Doré and Stewart, 2002).

10. Conclusion

The structural, petrological and geochronological investigation of the Austroalpine crust in the Southern Steep Belt allowed us to reconstruct the pre-Alpine evolution of the Languard-Tonale Tectono-Metamorphic Unit. The pre-D2 PT evolution indicates that the staurolite-bearing micaschists and sillimanite-bearing paragneisses belonged to two different tectono-metamorphic units. The PT evolution of the first unit is compatible with the thermal state of a continental upper plate during subduction or early collisional stages, and the second unit represents a thermal state of slab unrooting, which is consequential to the continental collision.

The two crustal slices coupled together during the D2 stage under granulite-

amphibolite facies conditions and formed a single tectono-metamorphic unit (Languard-Tonale Tectono-Metamorphic Unit). During this stage, the Permian acidic and basic intrusives were emplaced. D2 metamorphic conditions, which are suggested by mineral assemblages marking S2, indicate a high thermal regime that is compatible with an extensional tectonic setting and characterises the entire exhumation history of the Languard-Tonale Tectono-Metamorphic Unit.

Geochronological data constrains D2 at 275-250 Ma. This stage is part of the extensional tectonic regime responsible for the thinning of the Adriatic continental margin and the breakup of supercontinent Pangea from the Permian-Triassic to the Jurassic. Afterwards, the continental margin was tectonically reworked during the Alpine subduction and exhumation. The occurrence of pre-D2 subduction to collision-related metamorphic imprints indicates that this portion of the Austroalpine continental crust was thermally and mechanically perturbed by the Variscan convergence before the Permian thinning.

11. Acknowledgments

We gratefully acknowledge the Editor Marco Scambelluri, Eugenio Fazio and the anonymous reviewer for their highly constructive criticism of the text. Z.X. Li and W. Yao acknowledge the Australian Research Council's Laureat Fellowship grant to ZXL (FL150100133). This is a contribution to IGCP 648. M. Roda, M. Zucali and M.I. Spalla acknowledge Linea 2, Azione A - fondi giovani ricercatori "Evoluzione strutturale delle zone attive della litosfera e modellazione geodinamica" (PSR2015-1716DZANO-M). G. Gosso

is thanked for helpful discussion and critical reading of the text.

ACCEPTED MANUSCRIPT

- Auzanneau, E., Schmidt, M. W., Vielzeuf, D., D Connolly, J. A., 2010. Titanium in phengite: a geobarometer for high temperature eclogites. *Contributions to Mineralogy and Petrology* 159 (1), 1–24.
- Bertotti, G., Siletto, G., Spalla, M., 1993. Deformation and metamorphism associated with crustal rifting: The Permian to Liassic evolution of the Lake Lugano-Lake Como area (Southern Alps). *Tectonophysics* 226 (1-4), 271–284.
- Bigi, G., Castellarin, A., Coli, M., Dal Piaz, G., Sartori, R., Scandone, P., Vai, G., 1990. Structural Model of Italy, sheets 1-2: CNR, Progetto Finalizzato Geodinamica.
- Black, L. P., Kamo, S. L., Allen, C. M., Aleinikoff, J. N., Davis, D. W., Korsch, R. J., Foudouli, C., 2003. TEMORA 1: a new zircon standard for Phanerozoic U-Pb geochronology. *Chemical Geology* 200 (1), 155–170.
- Bockemuhl, C., Pfister, H., 1985. *Geologie der Serottini-Intrusion (Campo-Kristallin, Val Camonica, Italien)*. Schweizerische mineralogische und petrographische Mitteilungen 65 (1), 79–94.
- Bonsignore, G., Ragni, U., 1966. *Carta geologica dell'alta Valtellina e dell'alta Valcamonica*. Istituto di Mineralogia e Petrografia dell'Università di Milano.
- Bonsignore, G., Ragni, U., 1968. Contributo alla conoscenza del cristallino dell'alta Valtellina e dell'alta Val Camonica (Alpi Retiche) - Nota Prima: la formazione della P.ta di Pietra Rossa. *Fond. Probl. Mont. Ar. Alp. CNR* 73.

- Bousquet, R., Engi, M., Gosso, G., Oberhänsli, R., Berger, A., Spalla, M. I., Zucali, M., Goffè, B., 2004. Explanatory notes to the map: metamorphic structure of the Alps transition from the Western to the Central Alps. *Mitteilungen der Gesellschaft der Geologie- und Bergbaustudenten in Österreich* 149, 145–156.
- Braga, R., Giacomini, F., Messiga, B., Tribuzio, R., 2001. The sondalo gabbroic complex (central alps, Northern Italy): evidence for emplacement of mantle-derived melts into amphibolite-facies metapelites. *Physics and Chemistry of the Earth, Part A: Solid Earth and Geodesy* 26 (4–5), 333–342.
- Braga, R., Massonne, H.-J., Morten, L., dec 2007. An early metamorphic stage for the Variscan Ulten Zone gneiss (NE Italy): evidence from mineral inclusions in kyanite. *Mineralogical Magazine* 71 (6), 691–702.
- Brodie, K. H., Rex, D., Rutter, E. H., 1989. On the age of deep crustal extensional faulting in the Ivrea zone, Northern Italy. In: Coward, M. P.; Dietrich, D.; Park, R. G. (Ed.), *Alpine Tectonics*. Geological Society, London, Special Publications, pp. 203–210.
- Büchi, H., 1994. Der variskische Magmatismus in der stlichen Bernina (Graubünden, Schweiz). *Schweizerische Mineralogische Und Petrographische Mitteilungen* 74, 359–371.
- Cloos, M., 1993. Lithospheric buoyancy and collisional orogenesis: Subduction of oceanic plateaus, continental margins, island arcs, spreading ridges, and seamounts. *Geological Society of America Bulletin* 105 (6), 715.

- Coggon, R., Holland, T. J. B., 2002. Mixing properties of phengitic micas and revised garnet-phengite thermobarometers. *Journal of Metamorphic Geology* 20 (7), 683–696.
- Connolly, J., 2005. Computation of phase equilibria by linear programming: A tool for geodynamic modeling and its application to subduction zone decarbonation. *Earth and Planetary Science Letters* 236 (1-2), 524–541.
- Connolly, J. A. D., 1990. Multivariable phase diagrams: an algorithm based on generalized thermodynamics. *American Journal of Science* 290 (6), 666–718.
- Dal Piaz, G. V., 1993. Evolution of Austro-Alpine and Upper Penninic Basement in the Northwestern Alps from Variscan Convergence to Post-Variscan Extension. In: Raumer, J. F., Neubauer, F. (Eds.), *Pre-Mesozoic Geology in the Alps*. Springer Berlin Heidelberg, Berlin, Heidelberg, pp. 327–344.
- Dal Piaz, G. V., 2010. The Italian Alps: a journey across two centuries of Alpine geology. *Journal of the Virtual Explorer* 36 (8).
- Del Moro, A., Notarpietro, A., 1987. Rb-Sr geochemistry of some Hercynian granitoids overprinted by eo-alpine metamorphism in the Upper Valtellina, Central Alps. *Schweizerische Mineralogische und Petrographische Mitteilungen* 67, 295–306.
- Del Moro, A., Notarpietro, A., Potenza, R., 1981. Revisione del significato strutturale delle masse intrusive minori dell'alta Valtellina: risultati

- preliminari. *Rendiconti della Società Italiana di Mineralogia e Petrologia* 38 (1), 89–96.
- Diella, V., Spalla, M. I., Tunesi, A., 1992. Contrasting thermomechanical evolutions in the Southalpine metamorphic basement of the Orobic Alps (Central Alps, Italy). *Journal of Metamorphic Geology* 10 (2), 203–219.
- Doré, A. G., Stewart, I. C., 2002. Similarities and differences in the tectonics of two passive margins : the Northeast Atlantic Margin and the Australian North West Shelf. In: Keep, M., Moss, S. J. (Eds.), *The Sedimentary Basins of Western Australia 3*. Petroleum Exploration Society of Australia (PESA), pp. 89–117.
- England, P. C., Thomposon, A. B., 1984. Pressure–Temperature–Time Paths of Regional Metamorphism I. Heat Transfer during the Evolution of Regions of Thickened Continental Crust. *Journal of Petrology* 25 (4), 894–928.
- Ernst, W. G., Liou, J. G., 2008. High- and ultrahigh-pressure metamorphism: Past results and future prospects. *American Mineralogist* 93, 1771–1786.
- Froitzheim, N., Schmid, S. M., Conti, P., 1994. Repeated change from crustal shortening to orogen-parallel extension in the Austroalpine units of Graubuenden. *Eclogae Geologicae Helvetiae* 87 (2), 556–612.
- Gazzola, D., Gosso, G., Pulcrano, E., Spalla, M. I., 1997. Alpine deformation patterns and related mineral assemblages in the Languard-Campo root zone of Upper Valtellina. *Quad. Geod. Alp. Quat.* 4, 185–186.

- Gazzola, D., Gosso, G., Pulcrano, E., Spalla, M. I., 2000. Eo-Alpine HP metamorphism in the Permian intrusives from the steep belt of the central Alps (Languard-Campo nappe and Tonale Series). *Geodinamica Acta* 13, 149–167.
- Gerya, T., Stöckhert, B., 2006. Two-dimensional numerical modeling of tectonic and metamorphic histories at active continental margins. *International Journal of Earth Sciences* 95 (2), 250–274.
- Ghent, E. D., Stout, M. Z., 1981. Geobarometry and geothermometry of plagioclase-biotite-garnet-muscovite assemblages. *Contributions to Mineralogy and Petrology* 76 (1), 92–97.
- Gosso, G., Rebay, G., Roda, M., Spalla, M. I., Tarallo, M., Zanoni, D., Zucali, M., 2015. Taking advantage of petrostructural heterogeneities in subduction- collisional orogens , and effect on the scale of analysis. *Periodico di Mineralogia* 84 (3B), 779–825.
- Gosso, G., Salvi, F., Spalla, M. I., Zucali, M., 2004. Map of deformation partitioning in the polydeformed and polymetamorphic Austroalpine basement of the Central Alps (Upper Valtellina and Val Camonica, Italy). In: Pasquaré, G., Venturini, C., Groppelli, G. (Eds.), *Mapping Geology in Italy*. S.EL.CA., Firenze, pp. 292–301.
- Guntli, P., Liniger, M., 1989. Metamorphose in der Margna-Decke im Bereich Piz da la Margna und Piz Fedoz (Oberengadin). *Schweizerische Mineralogische Und Petrographische Mitteilungen* 69, 289–301.

- Handy, M. R., Franz, L., Heller, F., Janott, B., Zurrbruggen, R., 1999. Multistage accretion and exhumation of the continental crust (Ivrea crustal section, Italy and Switzerland). *Tectonics* 18 (6), 1154–1177.
- Henry, D. J., 2005. The Ti-saturation surface for low-to-medium pressure metapelitic biotites: Implications for geothermometry and Ti-substitution mechanisms. *American Mineralogist* 90 (2-3), 316–328.
- Holland, T. J., Powell, R., 1996. Thermodynamics of order-disorder in minerals. 2. Symmetric formalism applied to solid solutions. *American Mineralogist* 81, 1425–1437.
- Holland, T. J., Powell, R., 2001. Calculation of Phase Relations Involving Haplogranitic Melts Using an Internally Consistent Thermodynamic Dataset. *Journal of Petrology* 42 (4), 673–683.
- Holland, T. J. B., Powell, R., 1998. An internally consistent thermodynamic data set for phases of petrological interest. *Journal of Metamorphic Geology* 16 (3), 309–343.
- Kaneko, Y., Miyano, T., 2004. Recalibration of mutually consistent garnet-biotite and garnet-cordierite geothermometers. *Lithos* 73 (3), 255–269.
- Knig, M. A., 1964. Geologisch-petrographische Untersuchungen im oberen Veltlin. Ph.D. thesis, ETH, Zurich.
- Langone, A., Braga, R., Massonne, H.-J., Tiepolo, M., 2011. Preservation of old (prograde metamorphic) U-Th-Pb ages in unshielded monazite from the high-pressure paragneisses of the Variscan Ulten Zone (Italy). *Lithos* 127 (1-2), 68–85.

- Lardeaux, J.-M., 2014. Deciphering orogeny: a metamorphic perspective. Examples from European Alpine and Variscan belts: Part I: Alpine metamorphism in the western Alps. A review. *Bulletin de la Societe Geologique de France* 185 (2), 93–114.
- Lardeaux, J. M., Schulmann, K., Faure, M., Janoušek, V., Lexa, O., Skrzypek, E., Edel, J. B., Štípská, P., 2014. The Moldanubian Zone in the French Massif Central, Vosges/Schwarzwald and Bohemian Massif revisited: differences and similarities. *Geological Society, London, Special Publications* 405 (1), 7–44.
- Lardeaux, J. M., Spalla, M. I., 1991. From granulites to eclogites in the Sesia zone (Italian Western Alps): a record of the opening and closure of the Piedmont ocean. *Journal of Metamorphic Geology* 9 (1), 35–59.
- Ludwig, K. R., 2001a. Isoplot/Ex version 2.49 - A geochronological toolkit for Microsoft excel. Tech. rep., Berkeley Geochronological Centre Special Publication No. 1.
- Ludwig, K. R., 2001b. Squid version 1.02 - A geochronological toolkit for Microsoft excel. Tech. rep., Berkeley Geochronological Centre Special Publication No. 2.
- Mancktelow, N. S., Meier, A., Viola, G., Mller, W., Fgenschuh, B., Seward, D., Villa, I. M., 1999. The Periadriatic and adjacent fault systems in the Eastern Alps south and west of Tauern Window. In: *Abstr. of the 4th Workshop on Alpine Geol. Studies - Tbingen 21-24 Sept. 1999*. Tbinger Geowissenschaftliche Arbeiten, Series A, 52, pp. 7–9.

- Marotta, A. M., Roda, M., Conte, K., Spalla, M. I., 2018. Thermo-mechanical numerical model of the transition from continental rifting to oceanic spreading: the case study of the Alpine Tethys. *Geological Magazine* 155 (2), 250–279.
- Marotta, A. M., Spalla, M. I., 2007. Permian-Triassic high thermal regime in the Alps: Result of late Variscan collapse or continental rifting? Validation by numerical modeling. *Tectonics* 26 (4), 1–30.
- Marotta, A. M., Spalla, M. I., Gosso, G., 2009. Upper and lower crustal evolution during lithospheric extension: numerical modelling and natural footprints from the European Alps. In: Ring, U., Wernicke, B. (Eds.), *Extending a Continent: Architecture, Rheology and Heat Budget*. Vol. 321. The Geological Society, London, Special Publications, pp. 33–72.
- Meier, A., 2003. The Periadriatic fault system in Valtellina (N-Italy) and the evolution of the southwestern segment of the Eastern Alps. Ph.D. thesis, Swiss Federal Institute of Technology, ETH Zürich.
- Mohn, G., Manatschal, G., Beltrando, M., Masini, E., Kuszniir, N., 2012. Necking of continental crust in magma-poor rifted margins: Evidence from the fossil Alpine Tethys margins. *Tectonics* 31 (1), 1–28.
- Mohn, G., Manatschal, G., Masini, E., Müntener, O., 2011. Rift-related inheritance in orogens: a case study from the Austroalpine nappes in Central Alps (SE-Switzerland and N-Italy). *International Journal of Earth Sciences* 100 (5), 937–961.

- Newton, R. C., Charlu, T. V., Kleppa, O. J., 1980. Thermochemistry of the high structural state plagioclases. *Geochimica and Cosmochimica Acta* 44, 933–941.
- Perchuk, L. L., 1989. P-T -fluid regimes of metamorphism and related magmatism with specific reference to the granulite-facies Sharyzhalgay complex of Lake Baikal. Geological Society, London, Special Publications 43 (1), 275–291.
- Petri, B., Mohn, G., Skrzypek, E., Mateeva, T., Galster, F., Manatschal, G., 2017. U-Pb geochronology of the Sondalo gabbroic complex (Central Alps) and its position within the Permian post-Variscan extension. *International Journal of Earth Sciences*, 1–21.
- Petri, B., Mohn, G., Štípská, P., Schulmann, K., Manatschal, G., 2016. The Sondalo gabbro contact aureole (Campo unit, Eastern Alps): implications for mid-crustal mafic magma emplacement. *Contributions to Mineralogy and Petrology* 171 (5), 52.
- Pidgeon, R., Furfaro, D., Kennedy, A., Nemchin, A., van Bronswijk, W., Todt, W., 1994. Calibration of zircon standards for the Curtin SHRIMP II. In: *Eighth International Conference on Geochronology, Cosmochronology and Isotope Geology*. p. 251.
- Polino, R., Dal Piaz, G. V., Gosso, G., 1990. Tectonic erosion at the Adria margin and accretionary processes for the Cretaceous orogeny of the Alps. *Mémoires de la Société Géologique de France* 156, 345–367.

- Powell, R., Holland, T. J., 1999. Relating formulations of the thermodynamics of mineral solid solutions: Activity modeling of pyroxenes, amphiboles, and micas. *American Mineralogist* 84, 1–14.
- Regis, D., Rubatto, D., Darling, J., Cenko-Tok, B., Zucali, M., Engi, M., 2014. Multiple Metamorphic Stages within an Eclogite-facies Terrane (Sesia Zone, Western Alps) Revealed by Th-U-Pb Petrochronology. *Journal of Petrology* 55 (7), 1429–1456.
- Regorda, A., Roda, M., Marotta, A. M., Spalla, M. I., 2017. 2-D numerical study of hydrated wedge dynamics from subduction to post-collisional phases. *Geophysical Journal International* 211 (2), 952–978.
- Roda, M., Spalla, M. I., Marotta, A. M., 2012. Integration of natural data within a numerical model of ablative subduction: a possible interpretation for the Alpine dynamics of the Austroalpine crust. *Journal of Metamorphic Geology* 30 (9), 973–996.
- Salvi, F., Spalla, M. I., Zucali, M., Gosso, G., 2010. Three-dimensional evaluation of fabric evolution and metamorphic reaction progress in polycyclic and polymetamorphic terrains: a case from the Central Italian Alps. *Geological Society, London, Special Publications* 332, 173–187.
- Schaltegger, U., 1994. Unravelling the pre-Mesozoic history of Aar and Gotthard massifs (Central Alps) by isotopic dating : a review. *Schweizerische Mineralogische Und Petrographische Mitteilungen* 74, 41–51.
- Schmid, S. M., Berger, A., Davison, C., 1996. The Bergell pluton (Southern Switzerland, Northern Italy): overview accompanying a geological-tectonic

- map of the intrusion and surrounding country rocks. *Schweizerische Mineralogische Und Petrographische Mitteilungen* 76 (3), 329–355.
- Schuster, R., Scharbert, S., Abart, R., Frank, W., 2001. Permo-Triassic extension and related HT/LP metamorphism in the Austroalpine-Southalpine realm. *Mitt. Ges. Geol. Bergbaustud. Oesterr.* 45, 111–141.
- Schuster, R., Stüwe, K., 2008. Permian metamorphic event in the Alps. *Geology* 36, 603–606.
- Spalla, M. I., Gosso, G., 1999. Pre-Alpine tectonometamorphic units in the Central Southern Alps: structural and metamorphic memory. *Memorie Scienze Geologiche* 51 (1), 221–229.
- Spalla, M. I., Gosso, G., Marotta, A. M., Zucali, M., Salvi, F., 2010. Analysis of natural tectonic systems coupled with numerical modelling of the polycyclic continental lithosphere of the Alps. *International Geology Review* 52 (10-12), 1268–1302.
- Spalla, M. I., Lardeaux, J. M., Piazz, G. v. D., Gosso, G., Messiga, B., 1996. Tectonic significance of Alpine eclogites. *Journal of Geodynamics* 21 (3), 257–285.
- Spalla, M. I., Marotta, A. M., 2007. P-T evolutions vs. numerical modelling: a key to unravel the Paleozoic to early-Mesozoic tectonic evolution of the Alpine area. *Periodico di Mineralogia* 76 (2-3), 267–308.
- Spalla, M. I., Messiga, B., Gosso, G., 1995. LT-Alpine overprint on the HT rifting-related metamorphism in the steep belt of the Languard-Campo

- Nappe. The Cima Rovaia and Scisti del Tonale Units represent two different extents of Alpine re-equilibration. In: International Ophiolite Symposium. p. 148.
- Spalla, M. I., Siletto, G. B., di Paola, S., Gosso, G., 2000. The role of structural and metamorphic memory in the distinction of tectono-metamorphic units: the basement of the Como lake in the Southern Alps. *Journal of Geodynamics* 30 (1-2), 191–204.
- Spalla, M. I., Zanoni, D., Marotta, A. M., Rebay, G., Roda, M., Zucali, M., Gosso, G., 2014. The transition from Variscan collision to continental break-up in the Alps: insights from the comparison between natural data and numerical model predictions. Geological Society, London, Special Publications 405 (1), 363–400.
- Spalla, M. I., Zucali, M., 2004. Deformation vs. metamorphic re-equilibration heterogeneities in polymetamorphic rocks: a key to infer quality P-T-d-t path. *Rivista Italiana di Mineralogia e Petrologia* 73, 249–257.
- Spalla, M. I., Zucali, M., Di Paola, S., Gosso, G., 2005. A critical assesment of the tectono-thermal memory of rocks and definition of the tectonometamorphic units: evidence from fabric and degree of metamorphic transformations. In: *Deformation Mechanisms, Rheology and Tectonics: from Minerals to the Lithosphere*. Vol. 243. D. Gapais and J. P. Brun and P. Cobbold, pp. 227–247.
- Spalla, M. I., Zucali, M., Salvi, F., Gosso, G., Gazzola, D., 2003. Tectono-metamorphic map of the Languard-Campo, Serie del Tonale Nappes be-

- tween upper Val Camonica and Valtellina (Central Italian Alps, Austroalpine Domain). *Memorie Scienze Geologiche* 55, 105–118.
- Spear, F. S., 1993. *Metamorphic phase equilibria and Pressure-Temperature-time paths*. Min. Soc. Am. monograph., Washington.
- Spear, F. S., Cheney, J. T., 1989. A petrogenetic grid for pelitic schists in the system $\text{SiO}_2\text{-Al}_2\text{O}_3\text{-FeO-MgO-K}_2\text{O-H}_2\text{O}$. *Contributions to Mineralogy and Petrology* 101 (2), 149–164.
- Thoeni, M., 1981. Degree and evolution of the Alpine metamorphism in the Austroalpine Unit W of the Hohe Tauern in the light of K/Ar and Rb/Sr age determinations in micas. *Jahrbuch der Geologischen Bundesanstalt* 124, 111–174.
- Tribuzio, R., Thirwall, M. F., Messiga, B., 1999. Petrology, mineral and isotope geochemistry of the Sondalo gabbroic complex (Central Alps, Northern Italy): implications for the origin of post-Variscan magmatism. *Contributions to Mineralogy and Petrology* 136, 48–62.
- Venzo, S., Crespi, R., Schiavinato, G., Fagnani, G., 1971. Carta geologico-petrografica delle Alpi Insubriche Valtellinesi tra la Val Masino e la Val Malenco (Sondrio). *Memorie della Società Italiana di Scienze Naturali di Milano* 19.
- Viola, G., Mancktelow, N. S., Seward, D., Meier, A., Martin, S., 2003. The Pejo fault system: An example of multiple tectonic activity in the Italian Eastern Alps. *Geological Society of America Bulletin* 115 (5), 515–532.

- von Raumer, J. F., Bussy, F., Schaltegger, U., Schulz, B., Stampfli, G. M., 2013. Pre-Mesozoic Alpine basements-Their place in the European Paleozoic framework. *Geological Society of America Bulletin* 125 (1-2), 89–108.
- Werling, E., 1992. Tonale-, Pejo- und Judicarien-Linie: Kinematik, Mikrostrukturen und Metamorphose von Tektoniten aus räumlich interferierenden, aber verschiedenaltigen Verwerfungszonen. Ph.D. thesis, ETH, Zurich.
- White, R. W., Powell, R., Holland, T. J., Worley, B. A., 2000. The effect of TiO₂ and Fe₂O₃ on metapelitic assemblages at greenschist and amphibolite facies conditions: mineral equilibria calculations in the system: K₂O-FeO-MgO-Al₂O₃-SiO₂-H₂O-TiO₂-Fe₂O₃. *Journal of Metamorphic Geology* 18, 497–511.
- White, R. W., Powell, R., Holland, T. J. B., 2001. Calculation of partial melting equilibria in the system. *Journal of Metamorphic Geology* 19 (2), 139–153.
- Whitney, D. L., Evans, B. W., 2010. Abbreviations for names of rock-forming minerals. *American Mineralogist* 95, 185–187.
- Williams, I. S., 1997. U-Th-Pb geochronology by ion microprobe. In: McKibben W.C. Ridley, W. Ian, M. A. S. (Ed.), *Applications of microanalytical techniques to understanding mineralizing processes. Reviews in Economic Geology* 7. Society of Economic Geologists, pp. 1–35.
- Wu, C.-M., Zhang, J., Ren, L.-D., 2004a. Empirical Garnet-Biotite-

Plagioclase-Quartz (GBPQ) Geobarometry in Medium- to High-Grade Metapelites. *Journal of Petrology* 45 (9), 1907–1921.

Wu, C.-M., Zhang, J., Ren, L.-D., 2004b. Empirical garnet-muscovite-plagioclase-quartz geobarometry in medium- to high-grade metapelites. *Lithos* 78 (4), 319–332.

Zucali, M., 2001. La correlazione nei terreni metamorfici: due esempi dall'Austroalpino occidentale (Zona Sesia-Lanzo) e centrale (Falda Languard-Campo/ Serie del Tonale). Ph.D. thesis, Università degli Studi di Milano.

Zucali, M., Spalla, I., Gosso, G., 2002. Strain partitioning and fabric evolution as a correlation tool: the example of the Eclogitic Micaschists Complex in the Sesia-Lanzo Zone (Monte Mucrone-Monte Mars, Western Alps, Italy). *Schweiz. Mineral. Petrogr. Mitt.* 82, 429–454.

Figure 1: Structural sketch map of the Central Alps between upper Valtellina and Val Camonica redrawn after Venzo et al. (1971) and Bigi et al. (1990). Permian intrusives ages after Del Moro and Notarpietro (1987), Tribuzio et al. (1999), Braga et al. (2001) and Petri et al. (2017). Legend: AD=Adula; TA=Tambo'; SU=Suretta; PL=Platta; MA=Margna; M=Malenco; BE=Bernina; LCN=Languard-Campo Nappe; TS=Tonale serie; SA= Southalpine; ADm=Adamello pluton; ML=Mortirolo Line; PL=Periadriatic tectonic line.

Figure 2: Simplified geological map of the Mortirolo Pass area. Green and red colours represent the studied rocks that display pre-Alpine deformation history. Strongly Alpine metamorphosed rocks (white colour) consist of Wm-Gt-Chl-bearing micaschists, marble and calcisilicats, quartzites, amphibolites, orthogneiss and pegmatites all strongly affected by Alpine metamorphism. In the inset Schmidt stereographic projections, lower hemisphere are shown. Black star indicates the location of sample 04AP01 on which geochronological analysis has been performed. Coordinate system WGS 84 - UTM 32N.

Figure 3: a) Staurolite and Wm1a in staurolite-bearing micaschists outcrop. b) S1b and S2 foliations in sillimanite-bearing paragneisses outcrop. c) S2 foliation in sillimanite-bearing paragneisses marked by Bt1b and Grt1b. d) Contact between staurolite-bearing micaschists and Permian intrusive (granodiorite). S2 foliation does not affect the intrusive. e) Continuous S2 foliation in sillimanite-bearing paragneisses outcrop. f) Alpine S3 foliation occurring as axial plane to folds affecting S2 foliation in sillimanite-bearing paragneisses.

Figure 4: Detailed structural map of Passo Varadega (a) and Monte Serottini (b) areas. Color gradients in metapegmatites refers to the variation from coronitic (yellow) to mylonitic (red) fabric. Permian metapegmatites with igneous textures (a) and S2 pre-Alpine foliation still preserved within meter-size volumes, which partially escaped D3 Alpine deformation and metamorphism. During D4, centimeter to meter-size shear zones developed and mainly reactivated S3 shear zones (a) and open folds intersects S2 and S3 (b).

Figure 5: Microstructures in staurolite-bearing micaschists. a) S1a foliation marked by SPO of St, Wm1a and rare Bt1a. Relict of Ky is also detectable. LSP=3.3 mm. b) Grt1a rimmed by Grt_{ALP} and partially replaced by Sil2 in the core. LSP=3.3 mm. c) Wm_{ALP} marking D3 Alpine foliation with St porphyroblast. LSP=3.3 mm. d) St rimmed by And during post-D2 stage. LSP=6.0 mm.

Figure 6: Microstructures in sillimanite-bearing paragneisses. a) Sil1, Grt1b and Bt1b association characterising S1b foliation. LSP=3.3 mm. b) Sil1 and Bt1b association characterising S1b foliation. LSP=3.3 mm. c) Grt1b and Bt1b association characterising S1b foliation. LSP=3.3 mm. d) Garben of fibrolitic Sil2 replacing Bt1b and prismatic Sil1. LSP=3.3 mm.

Figure 7: Compositional variation of Bt in staurolite-bearing micaschists (a and b, eight different samples analysed) and sillimanite-bearing paragneisses (c and d, five different samples analysed). Bt1a has lower Ti content than Bt2 while Bt1b has higher Ti content than Bt2.

Figure 8: Compositional variation of Grt in staurolite-bearing micaschists (a, b, c and d, nine different samples analysed) and sillimanite-bearing paragneisses (e, f, g and h, six different samples analysed). Grt1 has a quite similar chemical composition within the both rocks. Grt_{ALP} has high Grs and low Alm content.

Figure 9: Compositional variation of Wm in staurolite-bearing micaschists (a, b and c, nine different samples analysed) and sillimanite-bearing paragneisses (d, e and f, four different samples analysed). A gradual decrease in Mg and Al content is observable from pre-Alpine to Alpine stage.

Figure 10: Pseudosections performed with Perple_X for staurolite-bearing micaschists (a) and sillimanite-bearing paragneisses (b). Wt% is reported. Variance fields: dark grey=5; grey=4; white=3. Red lines represent univariant curves. Light green and yellow boxes are referred to D1a and D1b stage respectively, pale green and orange are referred to D2 stage.

Figure 11: P-T-d history inferred from PT-estimates and pseudosections for both rocks (St-MS=staurolite-bearing micaschists, Sil-PG=sillimanite-bearing paragneisses, LT_{TMU}=Languard-Tonale Tectono Metamorphic Unit). Metamorphic facies after Ernst and Liou (2008): GS=greenschist; EA=epidote-bearing amphibolite; BS=blueschist; AM=amphibolite; Amp-EC=amphibole-bearing eclogite; HGR=high pressure granulite; GR=granulite. Geotherms: 1) near spreading ridge or volcanic arc and 2) normal gradient of old plate interior (Cloos, 1993); Vi=stable and V_∞=maximally relaxed geotherms (England and Thomposon, 1984) for continental crust.

Figure 12: Zircon U-Pb geochronology data for sample 04AP01: (a) concordia plot of 22 analyses with relatively concordant U-Pb ages; (b)-(c) concentrations of Permian metamorphic ages, (d) low-Th/U ratios from most of the dated Permian zircon rims illustrating a likely metamorphic origin, supported by their sector zoning structures in CL images (e-g).

Figure 13: Comparison between PT metamorphic conditions recorded by the two rock types, metamorphic field gradients and PT predictions recorded by crustal markers at different stages of a numerical model of Variscan convergence (from subduction to post-collisional stages, Regorda et al., 2017). V_o is the initial geotherm of the numerical model.

Table 1: Summary of the pre-Alpine deformation stages with characteristic structures and mineral associations.

Stage	Events	Structures	Mineral Association
		staurolite-bearing micaschists	
1	D1a, M1a	S1a composite foliation, from spaced to continuous	Bt1a+St+Wm1a+Grt1a+Pl+Qz+Rt+Ilm+Tur±Ky
2	D2, M2	S2 crenulation cleavage or spaced to continuous foliation	Bt2+Sil2+Pl+Qz+Tur±Grt1±Crd
post-2	Mpost2	Static growth of And	Wm2+Qz+Tur±And
		sillimanite-bearing paragneisses	
1	D1b, M1b	S1b spaced to continuous foliation	Bt1b+Sil1+Grt1b+Pl+Qz+Rt+Ilm±Kfs±Crd
post-1b	Mpost1b	Sill boudinage	Spl+Crn+Bt1 ₂
2	D2, M2	S2 from crenulation cleavage to spaced foliation	Bt2+Sil2+Pl+Ilm+Qz+Tur±Grt1±Crd
post-2	Mpost2	Static growth of And	Wm2+Qz+Tur±And

Table 2: Representative analysis of main minerals of staurolite-bearing micaschists.

Mineral	Bt 1a	Bt 2	Grt 1a	Grt 1 rim	St 1	Wm 1a	Wm 2	Pl	Ilm
SiO ₂	35.94	35.76	36.68	36.32	26.56	44.69	48.90	61.74	6.89
TiO ₂	1.61	2.61	0.14	0.07	0.37	0.27	0.42	0.00	41.89
Al ₂ O ₃	18.59	19.57	20.67	20.31	53.00	36.26	34.43	24.68	4.09
FeO	21.54	18.97	36.08	30.79	10.30	0.98	1.76	0.14	40.10
Fe ₂ O ₃	0.00	0.00	0.32	0.00	0.00	0.00	0.00	0.00	4.87
MnO	0.00	0.27	2.52	3.38	0.13	0.05	0.00	0.02	0.58
MgO	8.56	8.32	2.13	1.08	1.44	0.34	1.72	0.00	0.39
ZnO	0.00	0.00	0.16	0.00	2.25	0.00	0.05	0.04	0.00
CaO	0.12	0.00	1.11	7.06	0.03	0.04	0.00	5.95	1.07
Na ₂ O	0.86	1.03	0.00	0.56	0.00	2.27	0.73	8.12	0.54
K ₂ O	8.88	9.77	0.00	0.00	0.02	8.73	6.91	0.03	0.00
Sum	96.10	96.30	99.78	99.57	94.10	93.63	94.92	100.72	100.42
Ox	22.00	22.00	12.00	12.00	46.00	22.00	22.00	8.00	3.00
Si	5.47	5.40	2.99	2.96	7.64	6.03	6.39	2.72	0.17
Ti	0.18	0.30	0.01	0.00	0.08	0.03	0.04	0.00	0.75
Al	3.33	3.48	1.98	1.95	17.96	5.77	5.30	1.28	0.12
Fe ²⁺	2.74	2.39	2.46	2.10	2.48	0.11	0.19	0.01	0.81
Fe ³⁺	0.00	0.00	0.02	0.00	0.00	0.00	0.00	0.00	0.09
Mn	0.00	0.03	0.17	0.23	0.03	0.01	0.00	0.00	0.01
Mg	1.94	1.87	0.26	0.13	0.62	0.07	0.33	0.00	0.01
Zn	0.00	0.00	0.01	0.00	0.48	0.00	0.00	0.00	0.00
Ca	0.02	0.00	0.10	0.62	0.01	0.01	0.00	0.28	0.03
Na	0.25	0.30	0.00	0.09	0.00	0.59	0.18	0.69	0.03
K	1.72	1.88	0.00	0.00	0.01	1.50	1.15	0.00	0.00
Sum	15.67	15.66	8.01	8.10	29.30	14.11	13.59	4.99	2.01

Table 3: Representative analysis of main minerals of sillimanite-bearing paragneisses.

Mineral	Bt 1b	Bt 2	Grt 1b	Wm pre1b	Pl	Ilm	Crd	Spl
SiO ₂	34.11	35.41	37.17	45.22	57.14	0.53	57.46	0.00
TiO ₂	4.72	2.14	0.01	1.32	0.00	51.14	0.02	0.00
Al ₂ O ₃	18.29	20.16	21.56	34.18	27.50	0.43	32.04	61.59
FeO	21.52	18.53	35.76	1.28	0.55	43.29	6.80	26.92
Fe ₂ O ₃	0.00	0.00	0.00	0.00	0.00	0.00	0.00	4.57
MnO	0.03	0.00	1.69	0.02	0.06	4.29	0.07	0.87
MgO	6.00	8.27	2.25	0.60	0.03	0.07	6.26	2.56
ZnO	0.35	0.00	0.00	0.00	0.00	0.00	0.09	3.34
CaO	0.00	0.00	2.24	0.08	8.43	0.14	0.09	0.77
Na ₂ O	0.00	0.46	0.00	0.60	6.72	0.01	0.03	0.83
K ₂ O	9.95	9.00	0.01	11.18	0.06	0.19	0.02	1.14
Sum	94.94	94.02	100.69	94.60	100.49	100.09	102.88	102.13
Ox	22.00	22.00	12.00	22.00	8.00	3.00	18.00	32.00
Si	5.31	5.42	2.98	6.11	2.55	0.01	5.53	0.00
Ti	0.55	0.25	0.00	0.13	0.00	0.97	0.00	0.00
Al	3.36	3.64	2.04	5.44	1.45	0.01	3.64	15.92
Fe ²⁺	2.80	2.37	2.40	0.14	0.02	0.91	0.55	4.94
Fe ³⁺	0.00	0.00	0.00	0.00	0.00	0.00	0.00	0.75
Mn	0.00	0.02	0.11	0.00	0.00	0.09	0.01	0.16
Mg	1.39	1.89	0.27	0.12	0.00	0.00	0.90	0.84
Zn	0.04	0.00	0.00	0.00	0.00	0.00	0.01	0.54
Ca	0.00	0.00	0.19	0.01	0.40	0.00	0.01	0.18
Na	0.01	0.14	0.00	0.16	0.58	0.00	0.01	0.36
K	1.98	1.76	0.00	1.93	0.00	0.01	0.00	0.32
Sum	15.44	15.46	8.00	14.07	5.02	2.00	10.65	24.00

Table 4: Details on compositional variations in minerals marking different metamorphic stages of staurolite-bearing micaschists.

Mineral	D1a	D2	post-2
Bt	Ti=0.13-0.27	Ti=0.22-0.30	
	Al _{VI} =0.60-0.93	Al _{VI} =0.43-0.98	
	X _{Mg} =0.36-0.60	X _{Mg} =0.44-0.53	
Grt	Mg=0.06-0.50	Mg=0.12-0.22	
	Fe ²⁺ =1.59-2.47	Fe ²⁺ =1.80-2.25	
	Ca=0.03-0.82	Ca=0.44-0.67	
	Mn=0.01-0.66	Mn=0.03-0.35	
St	Al _{tot} =16.60-18.22		
	X _{Mg} =0.06-0.21		
	Zn=0.01-0.89		
Wm	Si=5.98-6.18		Si=6.06-6.45
	Ti=0.01-0.09		Ti=0.01-0.06
	Al _{tot} =5.55-5.93		Al _{tot} =4.98-5.70
	Mg=0.04-0.16		Mg=0.08-0.37
	Pg=0.00-0.32		Pg=0.00-0.25
Pl		X _{ab} =0.43-0.99	
		X _{an} =0.10-0.52	
		X _{san} =0.00-0.06	
Kfs		X _{ab} =0.75-0.80	
		X _{an} =0.03-0.06	
		X _{san} =0.15-0.22	
Ilm	Fe ²⁺ =0.81-1.00		
	Mg=0.00-0.01		
	Mn=0.00-0.04		

Table 5: Details on compositional variations in minerals marking different metamorphic stages of sillimanite-bearing paragneisses.

Mineral	D1b	post-1b	D2	post-2
Bt	Ti=0.38-0.57	Ti=0.00-0.08	Ti=0.20-0.39	
	Al _{VI} =0.46-0.97	Al _{VI} =1.34-2.38	Al _{VI} =0.66-1.36	
	X _{Mg} =0.27-0.42	X _{Mg} =0.31-51	X _{Mg} =0.27-0.45	
Grt	Mg=0.19-0.39			
	Fe ²⁺ =2.04-2.48			
	Ca=0.09-0.24			
	Mn=0.06-0.64			
Wm				Si=6.27-6.37
				Ti=0.06-0.18
				Al _{tot} =4.91-4.95
				Mg=0.34-0.37
Pl				Pg=0.01-0.04
			X _{ab} =0.15-0.82	
			X _{an} =0.18-0.85	
Kfs	X _{ab} =0.07-0.08			
	X _{an} =0.00			
	X _{san} =0.92-0.93			
Ilm	Fe ²⁺ =0.76-0.96			
	Mg=0.00-0.05			
	Mn=0.01-0.09			
Crd	Fe=0.55			
	Mg=0.90			
	Mn=0.01			
Spl		Fe ²⁺ =0.55-0.82		
		X _{Fe} =0.71-0.84		
		X _{Al} =0.99-1.00		

Table 6: Thermobarometric estimates for the rocks. References: Bt-Grt between 0.7 and 1.1 GPa (Kaneko and Miyano, 2004); Ti-Biotite (Henry, 2005); Grt-St between 0.7 and 1.1 GPa (Perchuk, 1989); GASP (Holland and Powell, 1998); GBPQ (Wu et al., 2004a); GPMB (Ghent and Stout, 1981); GMPQ (Wu et al., 2004b); Av. PT (Holland and Powell, 1998).

Lithotypes	Stage	Temperature (°C)				Pressure (GPa)				
		Ti-Biotite	Bt-Grt	Grt-St	Av. PT	GASP	GBPQ	GPMB	GMPQ	Av. PT
St-micaschists	D1a	567.0±33.9	564.5±32.6	559.4±30.0	654.5±38.8	0.73±3.2	0.63±1.4	0.75±2.6	0.57±0.9	0.85±1.8
	D2	629.6±19.9								
SH-paragneisses	D1b	711.6±11.2	654.3±22.7		663.0±156.0	0.42±1.3	0.41±1.0			0.60±2.2
	D2	653.4±35.5								

Table 7: SHRIMP zircon U-Pb data for Sample 04AP01. f_{206} (%) means the percentage of common ^{206}Pb in total Pb. Numbers in *Italic* are excluded from further analyses due to high common ^{206}Pb and/or high discordance

Spot	Th (ppm)	U (ppm)	Th/U	f_{206} (%)	$^{207}\text{Pb}/^{206}\text{Pb}$	1σ	Corrected Ratio s	$^{207}\text{Pb}/^{235}\text{Pb}$	1σ	$^{206}\text{Pb}_i/^{238}\text{Pb}$	1σ	Corrected Ages (Ma)	$^{207}\text{Pb}/^{235}\text{Pb}$	1σ	Conc (%)	
04AP01-01	219	558	0.39	0.79	0.0518	0.0015	0.3580	0.0112	0.0007	0.0007	0.0007	311	8	315	4	101
04AP01-02	6	379	0.02	0.00	<i>0.0534</i>	0.0012	0.3225	0.0086	0.0007	0.0438	0.0007	284	7	276	4	97
04AP01-03	71	149	0.48	0.65	<i>0.0523</i>	0.0020	0.6532	0.0270	0.0014	0.0905	0.0014	510	17	559	8	109
04AP01-04	69	784	0.09	-0.02	0.0513	0.0008	0.3095	0.0065	0.0006	0.0437	0.0006	274	5	276	4	101
04AP01-05	13	504	0.03	0.12	0.0518	0.0011	0.3086	0.0078	0.0006	0.0432	0.0006	273	6	273	4	100
04AP01-06	6	325	0.02	0.89	0.0458	0.0021	<i>0.2490</i>	0.0120	0.0006	0.0394	0.0006	226	10	249	3	110
04AP01-07	17	352	0.05	-0.17	0.0525	0.0013	0.3080	0.0087	0.0006	0.0418	0.0006	269	7	264	4	98
04AP01-08	12	405	0.03	0.10	0.0526	0.0011	0.3213	0.0083	0.0006	0.0443	0.0006	283	6	280	4	99
04AP01-09	10	409	0.02	0.11	0.0525	0.0021	0.3142	0.0135	0.0007	0.0434	0.0007	277	10	274	4	99
04AP01-10	8	785	0.01	0.07	0.0488	0.0011	0.2670	0.0074	0.0006	0.0397	0.0006	240	6	251	4	104
04AP01-11	12	388	0.03	1.43	0.0541	0.0031	0.3099	0.0185	0.0006	0.0416	0.0006	274	14	263	4	96
<i>04AP01-12</i>	<i>21</i>	<i>332</i>	<i>0.06</i>	<i>1.61</i>	<i>0.0469</i>	<i>0.0034</i>	<i>0.1439</i>	<i>0.0106</i>	<i>0.0003</i>	<i>0.0222</i>	<i>0.0003</i>	<i>136</i>	<i>9</i>	<i>142</i>	<i>2</i>	<i>104</i>
04AP01-13	7	375	0.02	1.39	0.0474	0.0030	0.2732	0.0178	0.0006	0.0418	0.0006	245	14	264	4	108
04AP01-14	8	305	0.03	0.09	0.0489	0.0012	0.2909	0.0084	0.0006	0.0431	0.0006	259	7	272	4	105
04AP01-15	11	557	0.02	-0.05	0.0531	0.0009	0.3178	0.0071	0.0006	0.0434	0.0006	280	5	274	4	98
04AP01-16	14	325	0.04	0.29	0.0492	0.0015	0.2812	0.0100	0.0007	0.0415	0.0007	252	8	262	4	104
<i>04AP01-17</i>	<i>12</i>	<i>77</i>	<i>0.16</i>	<i>0.82</i>	<i>0.0351</i>	<i>0.0058</i>	<i>0.0927</i>	<i>0.0154</i>	<i>0.0004</i>	<i>0.0192</i>	<i>0.0004</i>	<i>90</i>	<i>14</i>	<i>122</i>	<i>3</i>	<i>136</i>
<i>04AP01-18</i>	<i>66</i>	<i>522</i>	<i>0.13</i>	<i>1.57</i>	<i>0.0370</i>	<i>0.0033</i>	<i>0.2239</i>	<i>0.0205</i>	<i>0.0007</i>	<i>0.0439</i>	<i>0.0007</i>	<i>205</i>	<i>17</i>	<i>277</i>	<i>4</i>	<i>135</i>
04AP01-19	124	835	0.15	0.13	0.0511	0.0008	0.3104	0.0065	0.0006	0.0441	0.0006	274	5	278	4	101
04AP01-20	130	640	0.20	0.19	0.0489	0.0009	0.2951	0.0069	0.0006	0.0438	0.0006	263	5	276	4	105
04AP01-21	23	363	0.06	-0.04	0.0539	0.0020	0.3298	0.0134	0.0007	0.0444	0.0007	289	10	280	4	97
04AP01-22	12	431	0.03	0.28	0.0512	0.0013	0.2985	0.0087	0.0006	0.0423	0.0006	265	7	267	4	101
04AP01-23	4	305	0.01	0.24	0.0529	0.0022	0.2900	0.0126	0.0006	0.0398	0.0006	259	10	252	4	97
04AP01-24	20	906	0.02	0.00	0.0500	0.0007	0.2901	0.0058	0.0006	0.0420	0.0006	259	5	265	4	103
04AP01-25	22	311	0.07	0.03	0.0576	0.0011	0.4906	0.0122	0.0010	0.0617	0.0010	405	8	386	6	95

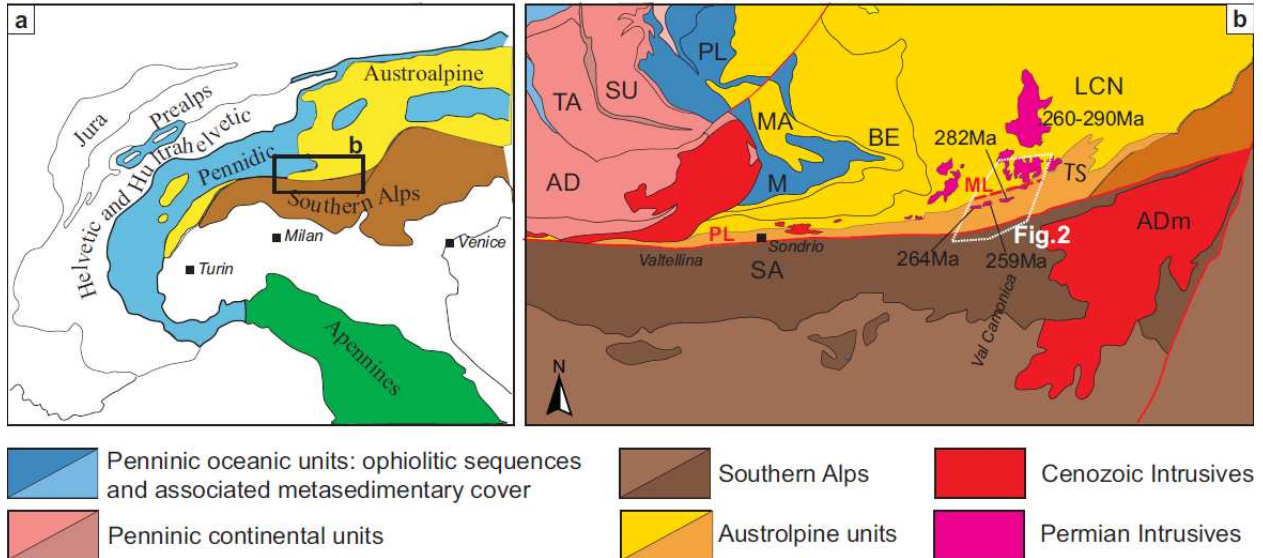


Fig. 1

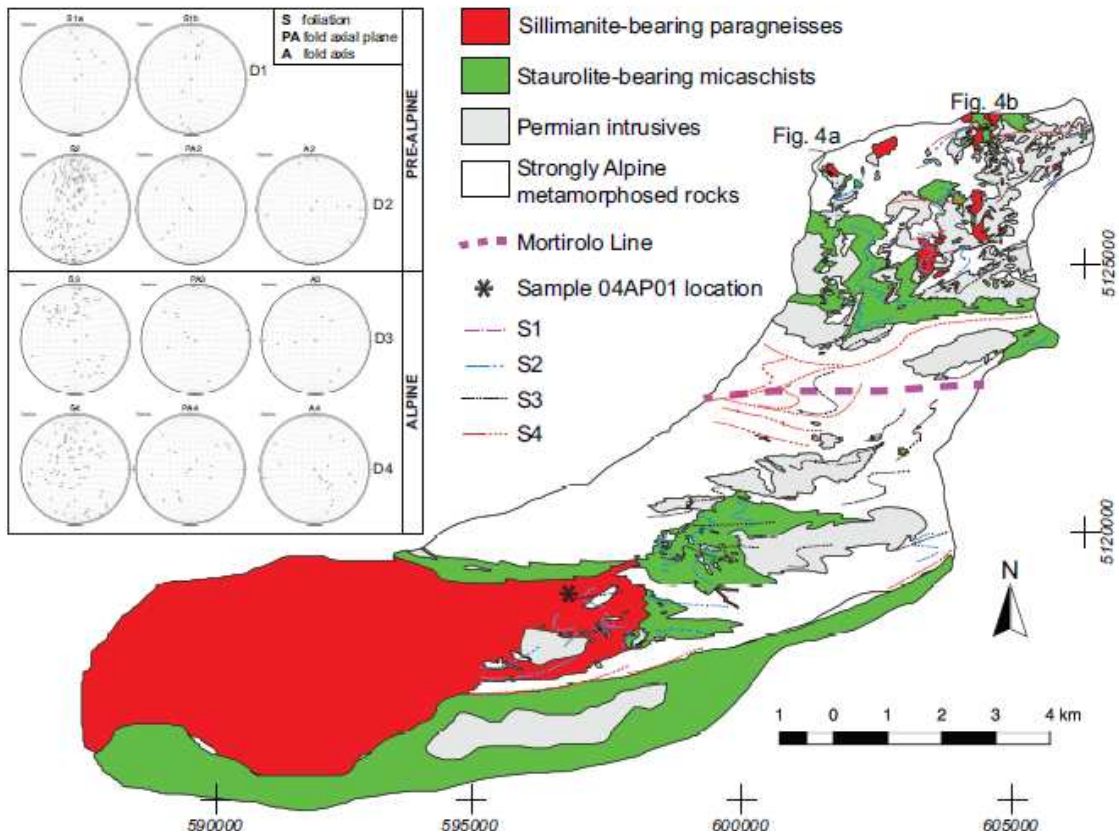


Fig. 2



Fig. 3

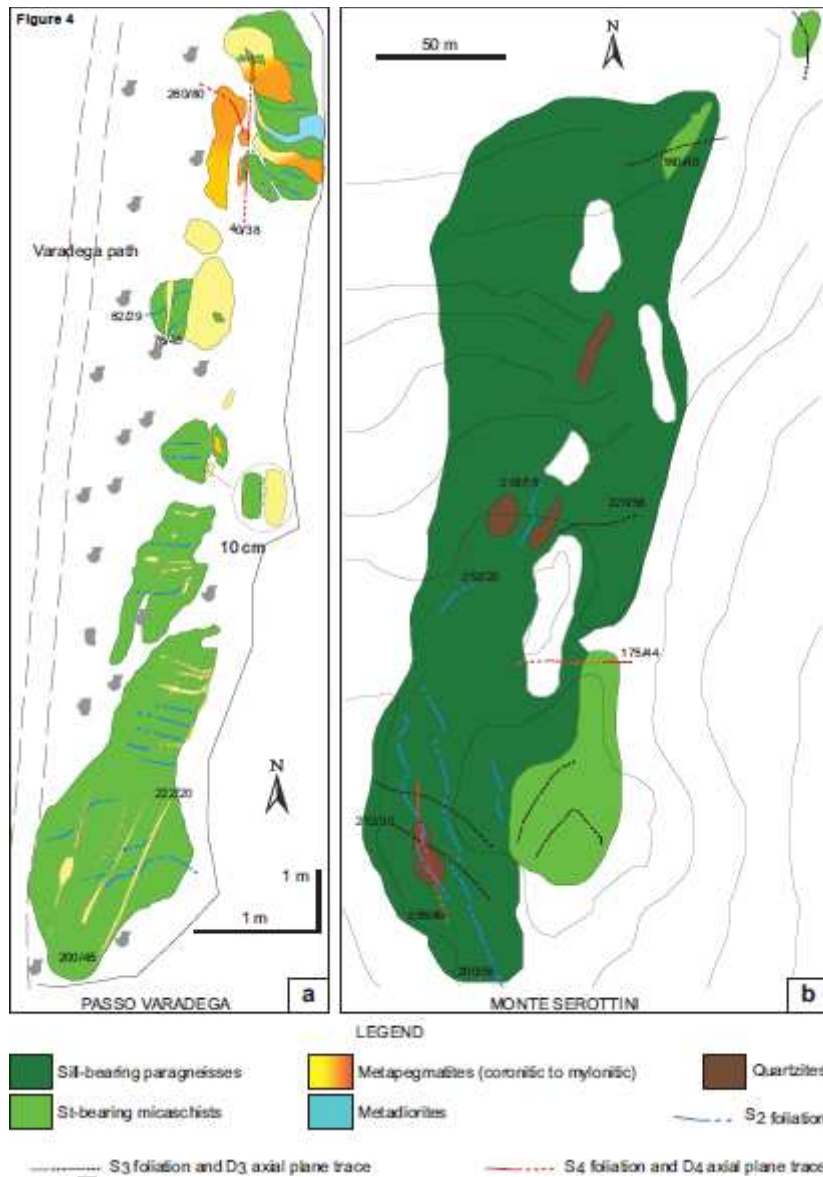


Fig. 4

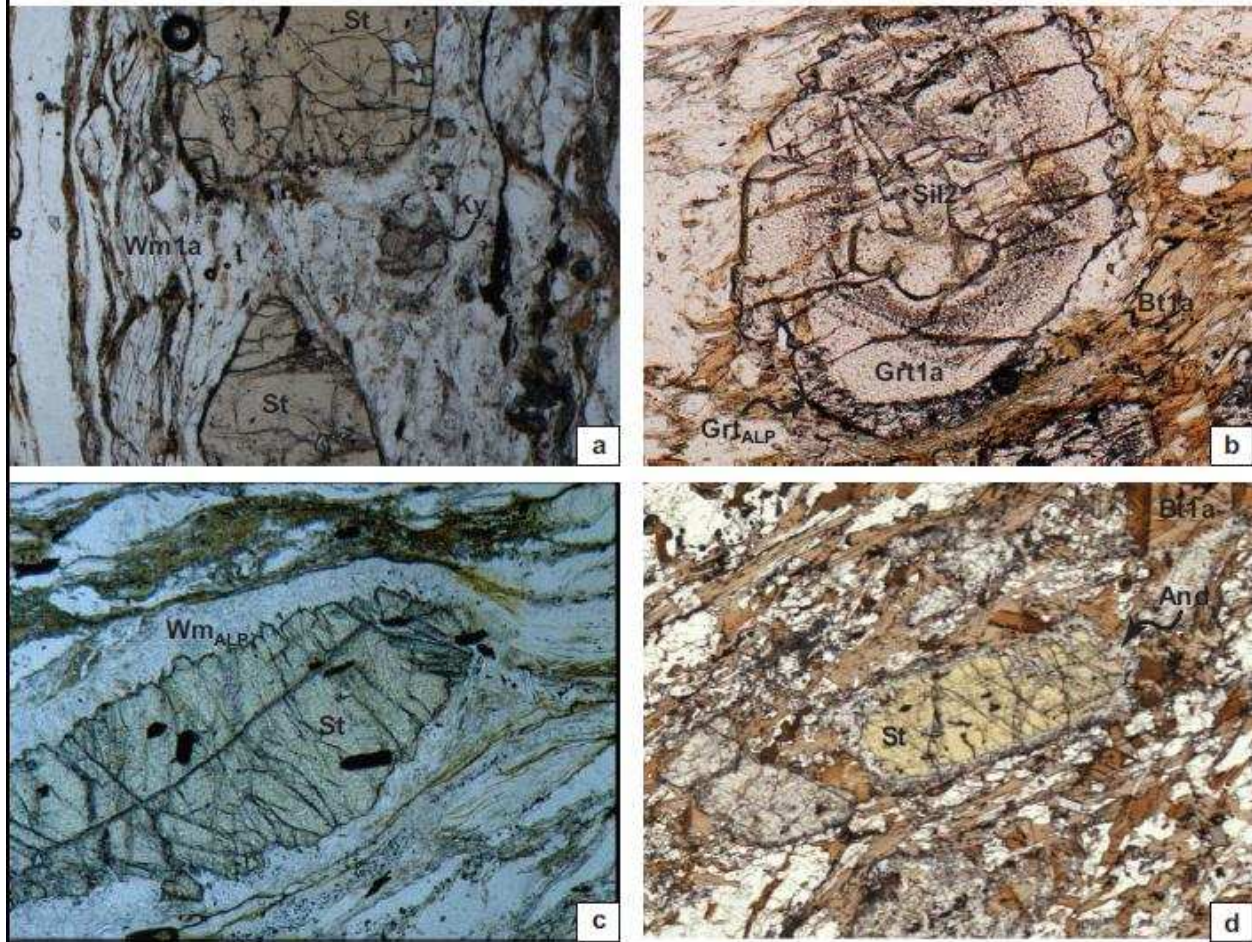


Fig. 5

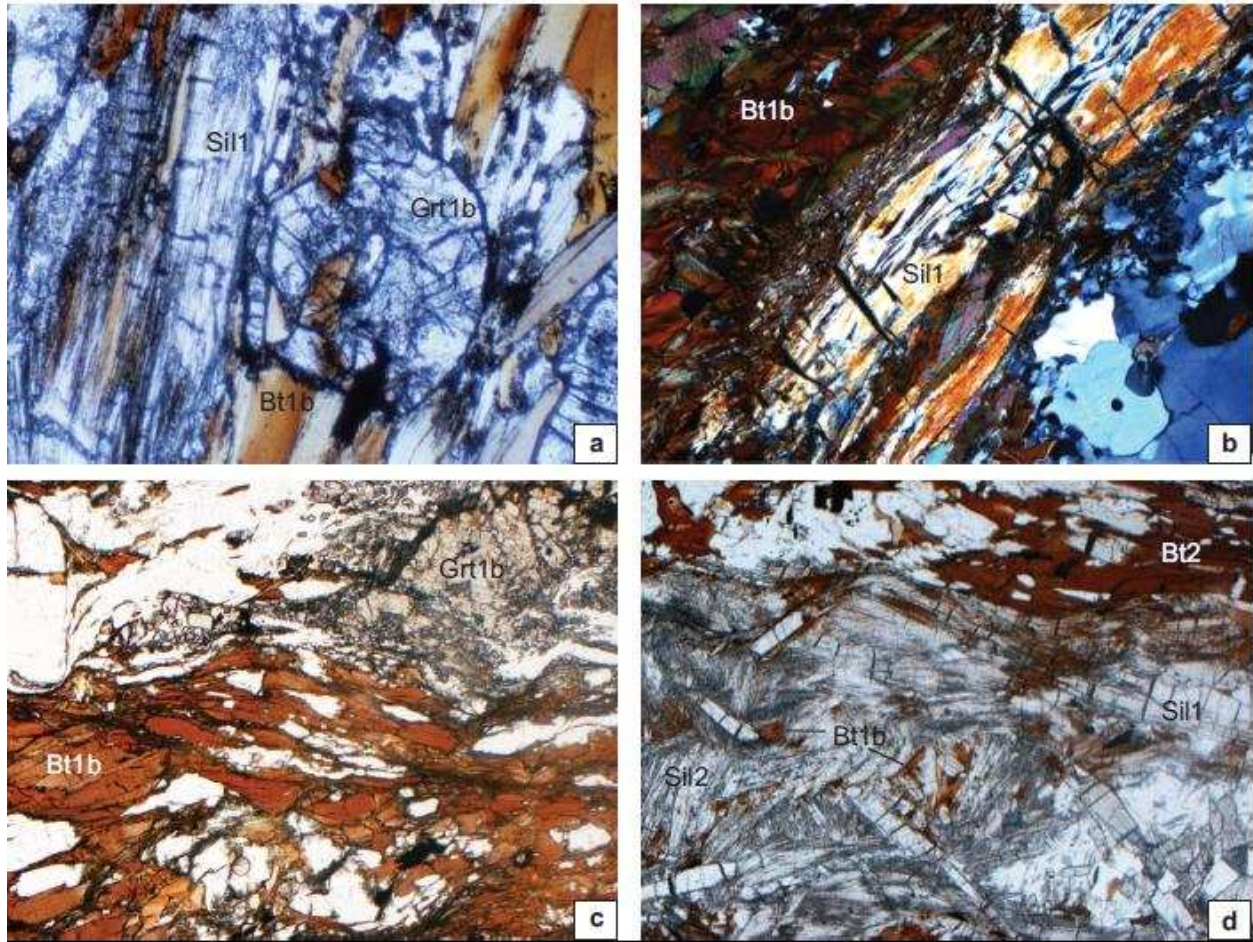


Fig. 6

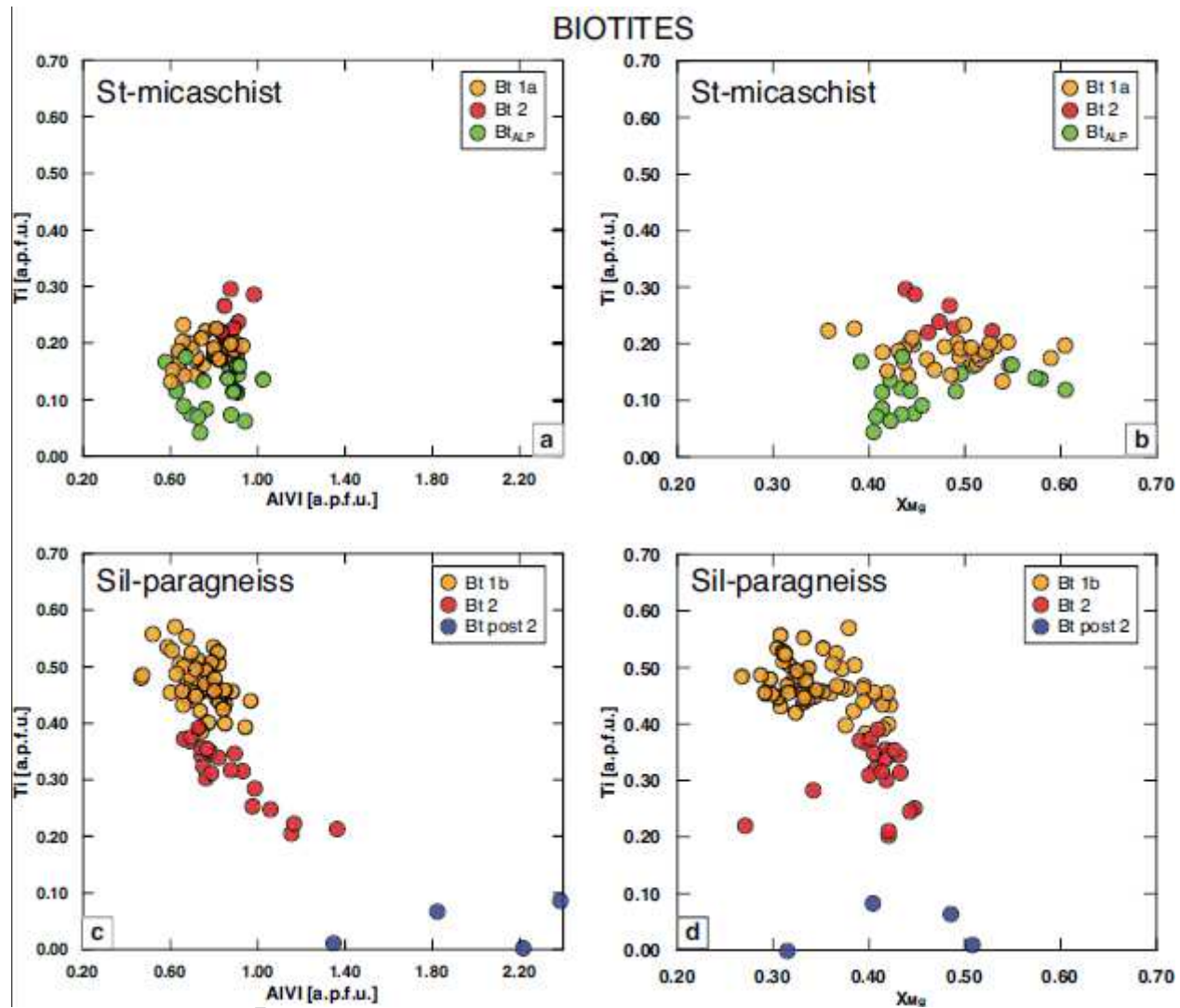


Fig. 7

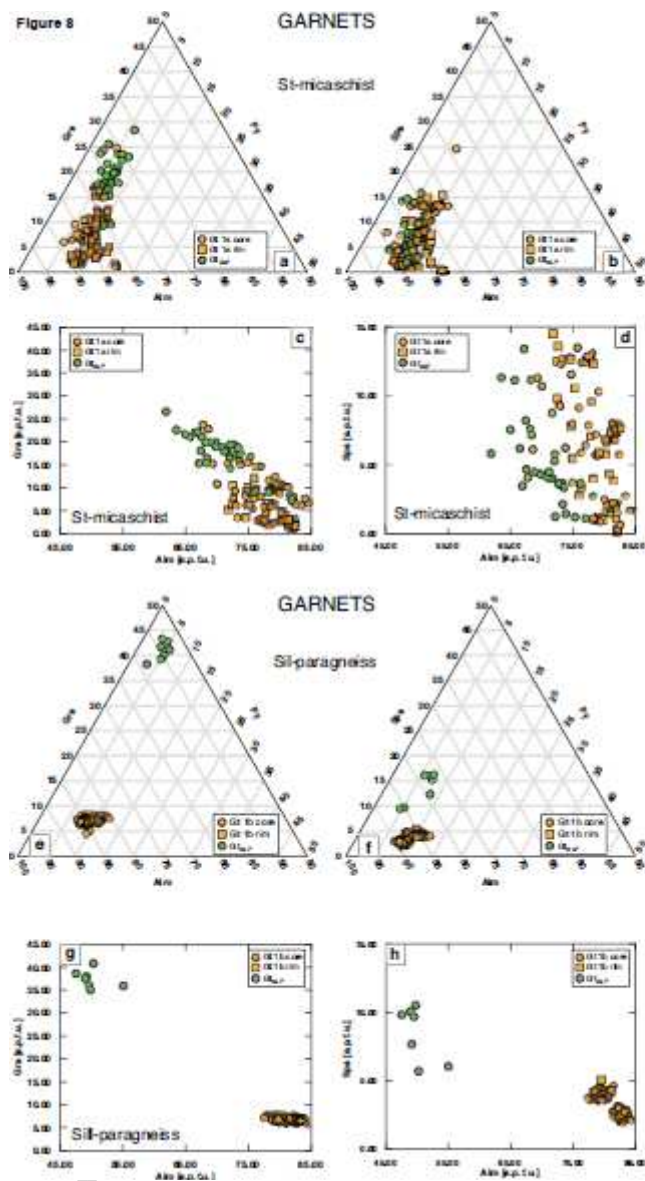


Fig. 8

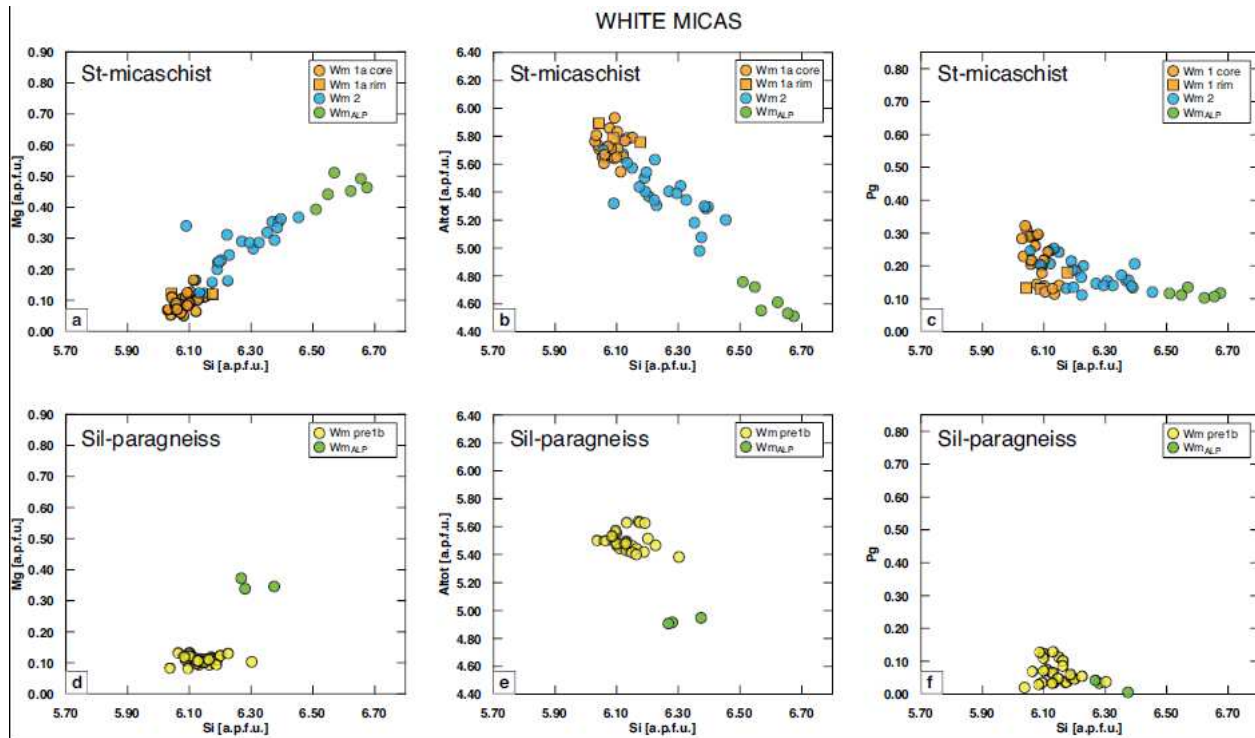


Fig. 9

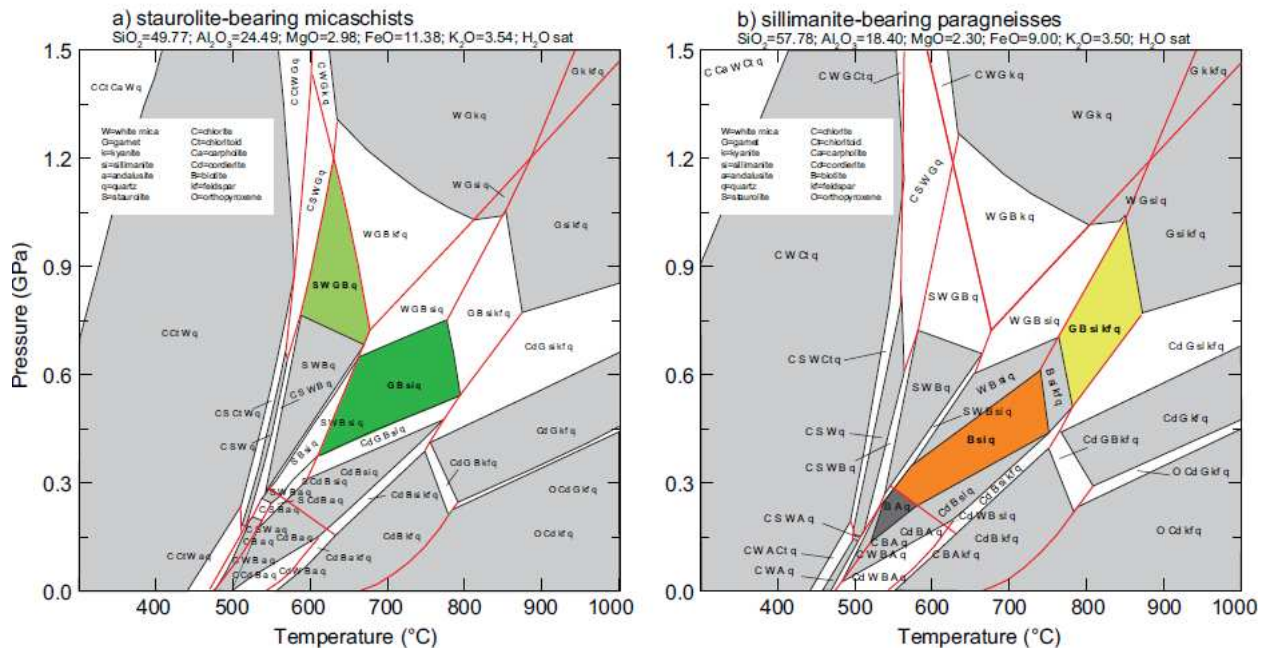


Fig. 10

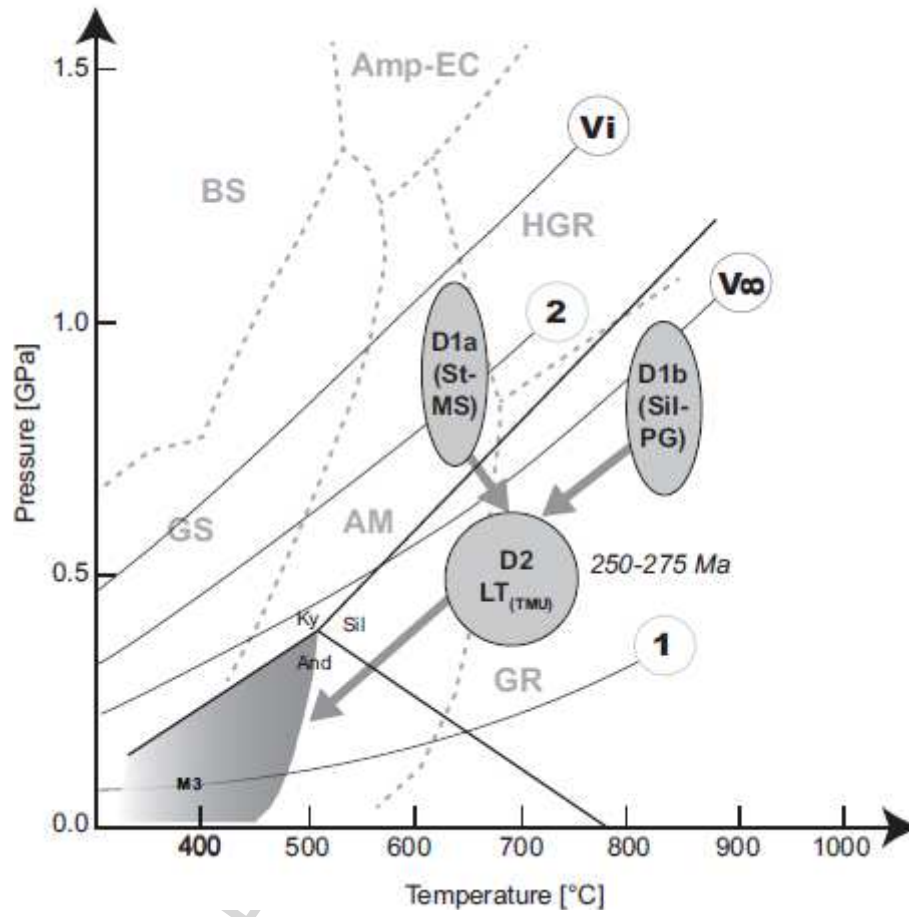


Fig. 11

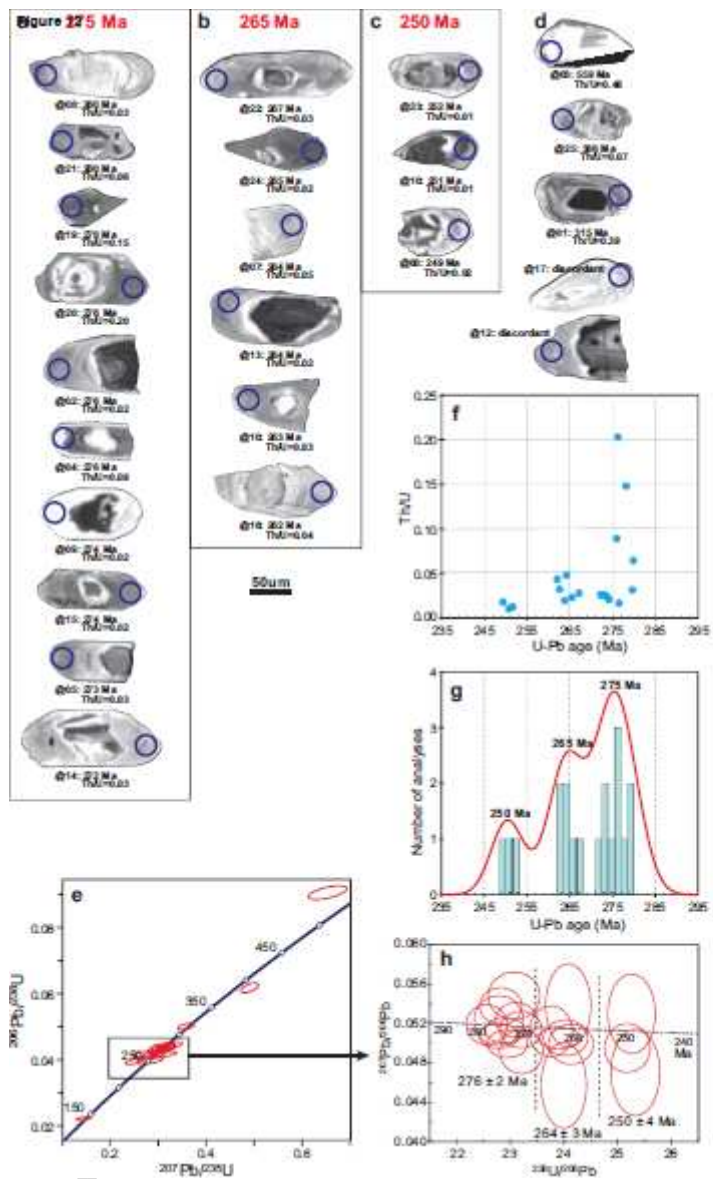


Fig. 12

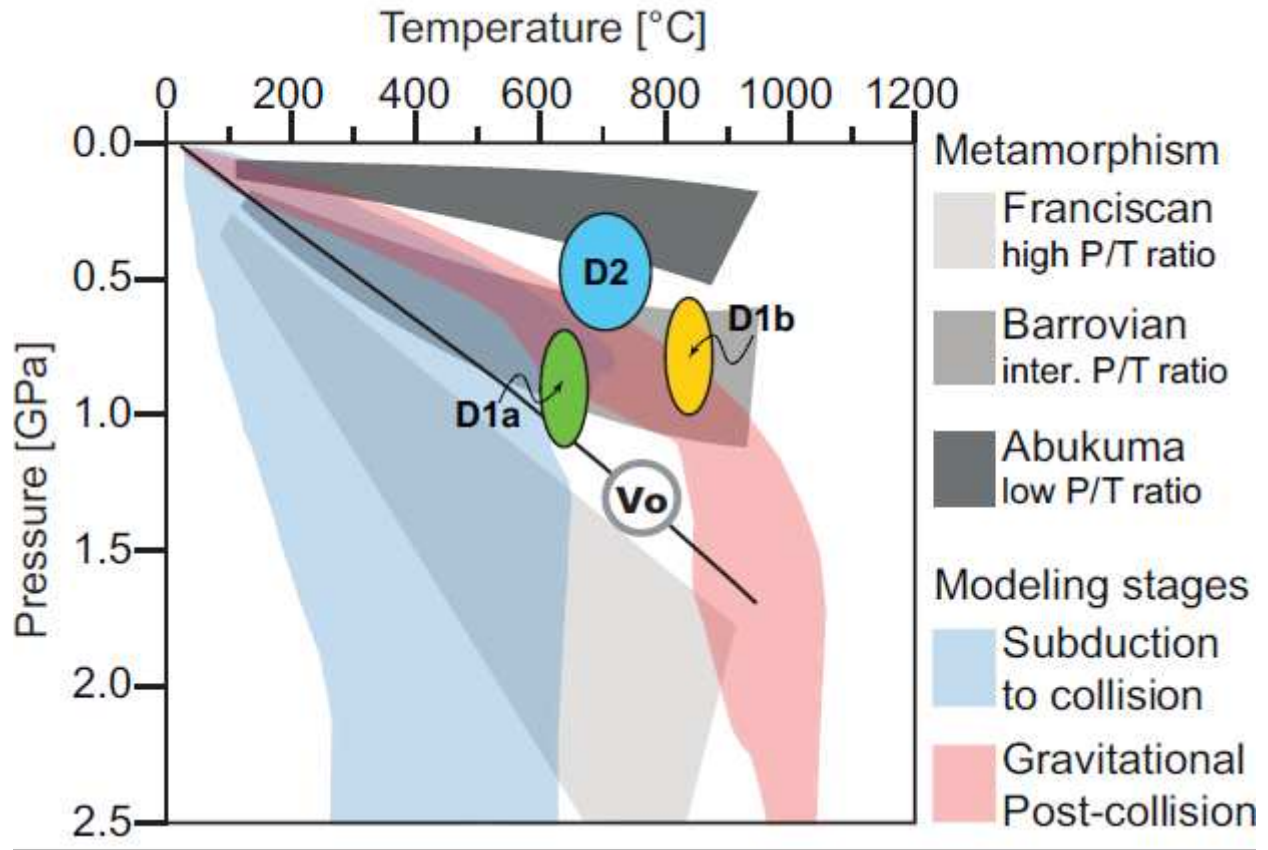


Fig. 13

Highlights

- We studied relicts of the pre-Alpine continental crust in the Southern Steep Belt.
- We reconstructed two different tectono-metamorphic units during D1.
- The two units became coupled during the second pre-Alpine stage (D2).
- This event is contemporaneous with the emplacement of Permian intrusives.
- D2 developed under a high thermal state compatible with extensional tectonic.